RADS Data Manual

Remko Scharroo

Version 4.6.2
10 April 2024

Contents

Chapter *1*

Introduction

This manual is intended to explain the details about the many variables available in the RADS data base. Many of the variables come in different "flavours", like one could choose to use the wet tropospheric correction based on radiometer measurements (wet_tropo_rad) or one of the atmospheric models (e.g., wet_tropo_ecmwf). RADS also provides the option to use more generic variable names (like wet_tropo) that will pick the best available correction depending on the satellite mission (or period).

The variables are organised by various chapters. Consult the table of contents to find the variables you are looking for, or go to the index at the end of the manual, where all variables are listed.

For each variable, a list of different flavours is presented. For an example, turn to Section 3.5. This Section describes the various wet tropospheric corrections. The table in that Section lists in the first column the various variable names, a short description, and the units of this variable. The field numbers as were used in RADS 3 (and can still be used in RADS 4) have been removed from this document in order not to give users the idea that they will be supported in perpetuity. The next column lists for which altimeter missions this variable is available (see Table 1.1), where "all" stands for all missions, and "other" stands for all missions not mentioned above it. The second to last column is the default range used for editing (NaN is returned when the value exceeds this range). When this column is empty, no range limits are set. Finally, the rightmost column relates to a list of notes provided in that Section.

Near the bottom of each variable table a number of "aliases" are provided. These are short-cuts to one (or more) of the flavours of variables. For example, the tables in Section 3.5 shows that for most altimeter missions the alias wet_tropo means that radiometer wet tropospheric correction is used (wet_tropo), but, when not available, for example during extended outage, the ECMWF model wet tropospheric correction (wet_tropo_ecmwf) is used instead. These "aliases" make it easier to get the preferred flavour of the variable which may differ from mission to mission (for example, some do not have a radiometer). This largely simplifies the construction of sea level anomalies, as described in Section 3.1.

Altimeter	Abbr.	Nr	Alternatives	Data origin (References)
GEOS 3	g3	1	ge3 geos-3 geos3	(not included in RADS)
Seasat	ss	2	sea seasat-a	(not included in RADS)
Geosat	gs	3	geo geosat	JGM-2 GDR [*Cheney et al.*, 1991]
ERS-1	e1	4	er1 ers-1 ers1	OPR2 [*Francis*, 1990; *Francis et al.*, 1991]
TOPEX	tx	5	top tpx topex	PO.DAAC GDR-F [*Rosmorduc et al.*, 2023]
Poseidon	pn	6	pos poseidon	PO.DAAC GDR-F [*Rosmorduc et al.*, 2023]
ERS-2	e2	7	er2 ers-2 ers2	OPR2 [*Francis et al.*, 1995]
GFO	g1	8	gfo gfo-1 gfo1	NOAA GDR
Jason-1	j1	9	ja1 jason-1 jason1	CNES GDR-E [*Ménard et al.*, 2003]
Envisat	n1	10	en1 envisat	ESA GDR
Jason-2	j2	11	ja2 jason-2 jason2	CNES GDR-D [*Lambin et al.*, 2010]
CryoSat-2	c2	12	cs2 cryosat-2 cryosat2	ESA GOP L2 Baseline C [*Bouffard*, 2015]
SARAL	sa	13	srl saral altika	CNES GDR-F [*Bignalet-Cazalet et al.*, 2021]
Jason-3	j3	14	ja3 jason-3 jason3	CNES GDR-F
HY-2A	2a	15	h2a hy-2a hy2a	(not included in RADS)
Sentinel-3A	3a	16	s3a sentinel-3a sentinel3a sntnl-3a	EUMETSAT Level 2 Baseline 005
Sentinel-3B	3b	17	s3b sentinel-3b sentinel3b sntnl-3b	EUMETSAT Level 2 Baseline 005
Sentinel-6A	6a	18	s6a s6mf sentinel-6a sentinel-6mf sentinel6a sntnl-6a	EUMETSAT Level 2 Baseline F08 (*)
SWOT nadir	sw	19	swt swot	PO.DAAC GDR-F

(*) Sentinel-6 data comes in two "branches", one for the conventional low-resolution (LRM) data (6a) and one for the high-resolution (SAR) data (6a.hr). Users can download either one or both of the directories. For convenience, download or create also the link 6a.lr that points to 6a.

Table 1.1   Abbreviation and numbers used for the various altimeter missions.

Time and location

2.1   Time

Time in the RADS data sets is stored as 8-byte floats in UTC seconds since a given epoch (normally 1 January 1985 or 1 January 2000). RADS will automatically convert these values into a few common time scales, depending on which time variable is selected. However, irrespective of the time scale, the clock references to UTC, rather than an atomic clock, meaning that leap seconds may result in a duplication of measurement times. No provision has been made to avoid confusion between measurements made before and after a leap second.

The time corresponds to the moment of reflection of the radar pulse on the sea surface and is corrected for time tag biases.

Variable	name	units	sat	range	note
time_1985	time since 1985-01-01 00:00:00	s	all		
time_2000	time since 2000-01-01 00:00:00	s	all		
time_rel_eq	time relative to equator crossing	s	all		1
time_local_solar	local solar time	s	all		2
time_mjd	time since 1858-11-17 00:00:00	days	all		3
time_ymdhms	time formatted as ymdhms		all		4
time	*alias of* time_1985		all		5

Notes:

1. Time is negative prior to equator crossing, positive thereafter.

2. The local solar time is expressed as seconds since the start of the day.

3. Time in Modified Julian Days.

4. The variable time_ymdhms will produce a floating value of the type 20110908135001.536 for 8 Sep 2011 13:50:01.536 UTC.

5. No time limit is set by default. Can be controlled by the `--t` or `--ymd` flags on the command line.

6. A time tag bias (surplus) of 1.8 ms was removed from the time tags of ERS-1 as they occurred on the ESA OPR (Ocean Product) data product. Likewise, all time tags of ERS-2 were decreased by 1.3 ms. The orbital altitude and location has been adjusted accordingly.

2.2   Latitude and longitude

The position of the centre of the footprint of the measurement is given by its geographical longitude and latitude relative the TOPEX reference ellipsoid. Longitude is in degrees relative to the Greenwich meridian, positive measuring east. Latitude is in degrees relative to the equator, positive measuring north.

Variable	name	units	sat	range	note
lat	latitude	degrees north	all	-90 90	
lon	longitude	degrees east	all	-180 180	1

Note:

1. RADS will automatically adjust the values to be within the range specified. So, by default, longitudes are kept within the -180 to +180 range.

2.3   Orbital altitude

The orbital altitude is the height of the centre-of-mass of the satellite above the TOPEX reference ellipsoid (semi-major axis = 6378136.3 m, inverse flattening = 298.257) as computed by satellite orbit determination. Numerous solutions exist, based on varying combinations of tracking data or gravity field solutions, or computed at shorter or longer latency. Some "legacy solutions" (those that were provided on the original data products) are included for reference even when they have been long replaced by more accurate solutions.

The altitude is that of the centre-of-mass of the spacecraft, so corrections from the tracking devices (DORIS, GPS, PRARE, SLR) to the centre-of-mass, as well as motion of the centre-of-mass within the spacecraft are accounted for, and should also be accounted for when later subtracting the altimeter range referenced to the same point.

If the time tags on the original GDR data include a bias, the orbit has either been (re)interpolated at the *corrected* time tag, or a correction proportional to the orbital altitude rate has been applied.

Variable	name	units	sat	range	note
alt_jgm3	JGM-3 altitude	m	gs		1
alt_dgme04	DGM-E04 altitude	m	e1 e2		2
alt_cnes	CNES altitude	m	c2 n1		3
alt_pgs7777	PGS7777 altitude	m	g1		4
alt_ggm02c_itrf2000	GGM02c(ITRF2000) altitude	m	gs		5
alt_eiggl04s	EIGEN-GL04c altitude	m	j1		6
alt_gdrcp	GDR-C' altitude	m	g1 gs j1 j2 n1		7
alt_gps	GPS altitude	m	j1 j2 j3 6a		8
alt_eig6c	EIGEN-6C altitude	m	c2 n1		9
alt_eig6s2	EIGEN-6S2 altitude	m	j1 j2		9
alt_gdrd	CNES GDR-D altitude	m	c2 j1 j2 n1 sa		10
alt_std1204	GSFC/Std1204 altitude	m	j1 j2		11
alt_reaper	REAPER/COMBI altitude	m	e1 e2		12
alt_reaper_deos	REAPER/DEOS altitude	m	e1 e2		12
alt_reaper_gfz	REAPER/GFZ altitude	m	e1 e2		12
alt_reaper_esoc	REAPER/ESOC altitude	m	e1 e2		12
alt_std1404	GSFC/Std1404 altitude	m	j2		13
alt_gdre	CNES GDR-E altitude	m	c2 j1 j2		14
alt_slcci	GFZ/SLCCI altitude	m	e1 e2 j1 j2 n1 pn tx		15
alt_std1808	GSFC/Std1808 altitude	m	tx pn		16
alt_gdrf	CNES GDR-F altitude	m	3a 3b 6a j3 sa sw tx pn		17
alt	*alias of* alt_gdrf		3a 3b 6a j3 sa sw tx pn		18
alt	*alias of* alt_gdre alt_cnes		c2		18
alt	*alias of* alt_reaper alt_gfz		e1 e2		18
alt	*alias of* alt_pgs7777		g1		18
alt	*alias of* alt_gdrcp		gs		18
alt	*alias of* alt_gdre		j1		18
alt	*alias of* alt_gdre alt_gdrd		j2		18
alt	*alias of* alt_gdrd alt_gdrcp		n1		18

Notes:

1. JGM-3 [*Tapley et al.*, 1996] was the original gravity field solutions used by NASA for the orbit determination of Geosat and TOPEX/Poseidon that featured on the GDR products. Though the gravity field was tailored to the TOPEX orbit, it was generally regarded the best at the time and was hence also used more widely than just for TOPEX/Poseidon. The radial orbit accuracy of about 3 cm for TOPEX/Poseidon and 8 cm for Geosat has since been superseded by more up-to-date orbit solutions.

2. DGM-E04 was a gravity field model developed at the Delft University of Technology tailored to the ERS-1 and ERS-2 orbits and derived from the JGM-3 model. The model significantly improved the radial orbit accuracy to about 3.5 cm, better than any general purpose models available at the time [*Scharroo and Visser*, 1998].

3. CNES produces the operational and precise orbits for a number of satellites. Unfortunately, in RADS the CNES orbits are based on mix of gravity field solutions. The CNES orbits for the TOPEX/Poseidon mission feature on the GDRs and are based on the JGM-3 gravity field model [*Tapley et al.*, 1996]. The CNES orbits for CryoSat and Envisat are obtained from their respective GDR products and are based on the EIGEN-GL04c gravity field model [*Ablain et al.*, 2008].

4. PGS7777 is a NASA preliminary gravity field solution tailored to the Geosat and GFO satellite orbits. The NASA PGS7777 orbit solution for GFO [*Lemoine et al.*, 2006] is based on SLR data only as the GPS tracking system on GFO failed.

5. Orbit solutions created at NASA using the GGM02c gravity field and station coordinates in the ITRF2000 reference frame.

6. Orbits produced with the EIGEN-GL04c or EIGEN-GL04s gravity fields.

7. Orbits produced under strict Jason GDR-C' standards.

8. Reduced-dynamic orbits generated by NASA/JPL based on GPS tracking data only. Jason-1 Cycles 1-161 contain "Release 11a", Jason-2 Cycles 1-327 "Release 18a", Jason-3 Cycles 1-226 "Release 22a", Sentinel-6a Cycles 5-60 "Release 22a".

9. Orbits provided by ESOC using the EIGEN-6C or EIGEN-6S2 gravity field. The orbits are available for parts of the various altimeter missions only: CryoSat-2 cycles 4-58, Envisat all cycles, Jason-1 cycles 1-260, Jason-2 cycles 1-220.

10. Orbits produced by CNES under strict Jason GDR-D standards [*International DORIS Service*, 2011]. These orbits are kept on Jason-2 data (until April 2015) and SARAL data (until June 2015) for comparison, although the GDR-E orbits are now default. Jason-1 data does not have GDR-E orbits yet.

11. Orbits provided by GSFC using their standards "Std1204". They are "GDR-D compatible" and use the goce2s_fit2 gravity field [*Lemoine et al.*, 2013].

12. Orbits produced by the REAPER project. A combined solution and individual solutions created by DEOS (TU Delft), GFZ and ESOC are available [*Rudenko et al.*, 2011].

13. Orbits provided by GSFC using their standards "Std1404". They are "GDR-E compatible".

14. Orbits produced by CNES under strict Jason GDR-E standards (baseline for the production of orbits since April 2015) [*International DORIS Service*, 2015].

15. Orbits produced by GFZ in the framework of the ESA Sea Level CCI project. RADS initially included version VER06 of these orbits (based on the EIGEN-6S2A gravity field model) [*Rudenko et al.*, 2014] for ERS-1, ERS-2, Envisat and TOPEX/Poseidon. Any data produced since 18 May 2016 (which includes Jason-1 and Jason-2) incorporated version VER11 of these orbits and are based on the EIGEN-6S4 gravity field model [*Rudenko et al.*, 2015, 2016].

16. Orbits provided by GSFC for TOPEX and Poseidon reprocessing, using their standards "Std1808". They are "GDR-F compatible".

17. Orbits produced by CNES under strict Jason GDR-F/POE-F standards (baseline for the production of orbits since 2020).

18. The variable alt refers to the preferred (best) orbit solution for each satellite. If two variable names are mentioned, RADS picks the first one by preference; it that is not available, the second variable is used.

2.4　Orbital altitude rate

The rate of change of the orbital altitude is relevant for computing the Doppler correction and for correcting the altitude as a result of a time tag bias. Furthermore, the orbital altitude rate can be used to estimate time tag biases.

Variable	name	units	sat	range	note
alt_rate	orbital altitude rate	m/s	all		

Sea level variables

3.1   Sea level anomaly

The sea level anomaly (SLA) or sea surface height anomaly (SSHA) is the height for the sea surface relative to a long term mean. It can be constructed by subtracting from the satellite orbital altitude the altimeter range, propagation corrections, sea state bias, tides, and a mean sea surface model.

The sea level anomaly in RADS is always computed on-the-fly. This means that the RADS software will gather the required variables and their selected flavours from the netCDF data files, edit those data based on the user-selected criteria, and then constructs the sea level anomaly based on those. If any of the variables that make up the sea level anomaly is not available, marked invalid, or is out of range, then the sea level anomaly is also marked invalid (set to the NaN value). In addition, variables that do not strictly make up the sea level anomaly (like wave height or wind speed) can be used as edit criteria, e.g. rejecting data with high sea states.

The rads.xml configuration file spells out, in reverse polish notation (RPN), how the sea level anomaly (sla) is computed. The 'sea level equation' is written as:

```
<data>
    alt range SUB dry_tropo SUB wet_tropo SUB iono SUB
    dac SUB tide_solid SUB tide_ocean SUB tide_load SUB
    tide_pole SUB ssb SUB mss SUB ref_frame_offset SUB
</data>
```

where SUB stands for 'subtract' and the others are names or aliases of the various variables that make up the sea level anomaly. If any of these variables is NaN, the result is NaN as well. The use of aliases comes in handy here. We can, for example, switch out the orbit solution between one flavour and another simply by directing the alias alt from say alt_jgm3 to alt_dgme04. We do not have to change anything to the sea level equation.

The configuration file also spells out which variables are used as 'quality flag'. That is, if any of these variables is set to NaN, the sea level anomaly is also set to NaN, even though these variables are not added or subtracted as part of the 'sea level equation'. For example:

```
<quality_flag>
    swh sig0 range_rms range_numval flags
</quality_flag>
```

While the sea level anomaly variable sla is computed on-the-fly by the RADS software, there

is a second variable `ssha` that is already stored on the RADS products. Users can use this variable directly as well, but then give up the opportunity to edit the results themselves.

Variable	name	units	sat	range	note
sla	sea level anomaly	m	all	-5 5	1
ssha	sea level anomaly (precomputed)	m	all		2

Notes:

1. The limits on the sea level anomaly can be changed in the configuration file, of by using the `--sla=MIN,MAX` option on the command line.

2. The variable `ssha` is read directly from the RADS products and already is screened by editing.

3.2   Altimeter range

The range between the satellite and the sea surface is based on the total travel time of the radar pulse divided by twice the speed of light. This range is then corrected for internal paths within the instrument (internal calibration), variations in the frequency of the ultra-stable os-cillator (USO correction), and the distance between the antenna and the satellite centre of mass (centre-of-mass offset). The range is further corrected for the Doppler effect. As such the range measures the distance between the satellite centre of mass and the sea surface, except for path delays in the atmosphere and sea surface interactions.

To compute the height of the sea surface, we subtract the primary range (generally Ku-band) from the satellite orbital altitude and then further correct for path delays and other corrections.

Dual-frequency altimeters measure the range also on a secondary frequency (C- and S-band) which allows for the computation of the ionospheric path delay directly for altimeter observa-tions rather than models.

Variable	name	units	sat	range	note
range_ka	altimeter range (Ka)	m	sa		
range_ku	altimeter range (Ku)	m	other than sa		
range_ku_mle3	altimeter range (MLE3)	m	6a j2 j3 sw tx		8
range_ku_plrm	altimeter range (PLRM)	m	3a 3b c2		9
range_ku_adaptive	altimeter range (adaptive retracking)	m	j3 sw		10
range_ku_nr	altimeter range (numerical retracking)	m	3a 3b 6a		10
range_c	altimeter range (C)	m	j1 j2 j3 sw tx		7
range_s	altimeter range (S)	m	n1		6
range	*alias of* range_ka		sa		
range	*alias of* range_ku		other than sa		
range_ku_nr	*alias of* range_ku_adaptive		j3 sw		10

Notes:

1. A constant bias of -124 mm is added to the Geosat range. An additional internal calibration and USO correction comes from an external file [*Brian Beckley*, priv. comm., 2002].

2. The range of the ERS-1 and ERS-2 altimeters has been corrected for SPTR bias jumps and USO drift based on offline tables [*Martini and Féménias*, 2000].

3. A constant bias of 409.2 mm is added to the ERS-1 range [*Francis et al.*, 1993; *Stum et al.*, 1998].

4. The ERS-2 USO correction appears to be low during the periods 1997-07-26 20:24:04 to 1998-01-07 03:58:09 and 1998-03-17 11:10:48 to 2000-01-08 06:04:13. During both periods 4.77 mm is added to the USO correction (and to range).

5. The USO correction for Envisat is based on external USO correction files (1-Hz data): http://earth.esa.int/pcs/envisat/ra2/auxdata/

6. Even though the Envisat Ku- and S-band ranges have biases of the order of 45 cm, this is not corrected for in the range, but in the reference frame offset (ref_frame_offset). A correction of 150 mm is added to the S-band range to account for a bias in the dual-frequency ionosphere correction [*Scharroo and Smith*, 2010]. During the short operation of the Side B altimeter, an additional 9 mm was added to both Ku- and S-band ranges. S-band range for Envisat is available only until the loss of the S-band signal.

7. A constant bias of -2.3 mm is added to the Jason-1 C-band range to account for a bias in the dual-frequency ionosphere correction [*Scharroo and Smith*, 2010].

8. A separate range measurement based on the MLE3 retracker is available for Jason-2 and -3, as well as for Sentinel-6, SWOT and TOPEX.

9. For the SAR altimeters of Sentinel-3 and Cryosat-2, an LRM-like processing, known as PLRM (Pseudo Low Resolution Mode) is available.

10. The adaptive (for Jason-3 and SWOT) and numerical retracking (for Sentinel-6) replace the conventional MLE retracking. It is more accurate and better takes into account the change of the instrument's point target response (PTR). For convenience an alias range_ku_nr for range_ku_adaptive is provided.

3.3 Altimeter range statistics

The altimeter ranges are provided in RADS as (approximately) 1-second averages based on 10, 20, or 40 'elementary' measurements during that second. The altimeter range reported is, in fact, not the statistical mean, but is generally determined as follows:

- Interpolate the orbital altitude at the same time tags as the elementary measurements;
- Subtract the orbital altitude from the range;
- Fit a linear trend true 'range minus orbit';
- Remove the linear trend;
- Compute the standard deviation of the residuals (using $n - 2$ in the denominator) where n is the number of elementary measurements during a 1-Hz period;
- Evaluate the linear trend at the mid point and add the local orbital altitude back at this point to obtain the average range.

Hence, technically, range_rms is not the standard deviation of the altimeter range, but the standard deviation of the elementary 'orbit minus range' values with a trend fitted and removed as well, and taking into account the extra degree of freedom. It should also not be confused with an error estimate for the range measurement.

Variable	name	units	sat	range	note
range_rms_ka	std dev of Ka-band range	m	sa	0.0 0.17	
range_rms_ku	std dev of Ku-band range	m	g1 gs	0.0 0.25	
			6a j1 j2 j3 pn sw	0.0 0.17	
			c2	0.0 0.18	
			tx	0.0 0.15	
			other	0.0 0.4	
range_rms_ku_mle3	std dev of Ku-band range (MLE3)	m	6a j2 j3 sw tx	0.0 0.17	1
range_rms_ku_plrm	std dev of Ku-band range (PLRM)	m	3a 3b c2	0.0 0.17	2
range_rms_ku_adaptive	std dev of Ku-band range (adap.)	m	j3 sw	0.0 0.17	3
range_rms_ku_nr	std dev of Ku-band range (NR)	m	6a	0.0 0.17	3
range_rms_c	std dev of C-band range	m	j1 j2 j3 sw	0.0 0.4	
range_rms_s	std dev of S-band range	m	n1	0.0 0.4	4
range_rms	*alias of* range_rms_ka		sa		
range_rms	*alias of* range_rms_ku		other than sa		
range_rms_ku_nr	*alias of* range_rms_ku_adaptive		j3 sw		3
range_numval_ka	nr of valid Ka-band ranges		sa	33 40	
range_numval_ku	nr of valid Ku-band ranges		g1 gs	9 10	
			6a j1 j2 j3	16 20	
			sw tx pn	16 20	
			3a 3b	17 21	5
			other	17 20	
range_numval_ku_mle3	nr of valid Ku-band ranges (MLE3)		6a j2 j3 sw tx	16 20	1
range_numval_ku_plrm	nr of valid Ku-band ranges (PLRM)		3a 3b c2	17 21	2
range_numval_ku_adaptive	nr of valid Ku-band ranges (adap.)		j3 sw	16 20	3
range_numval_ku_nr	nr of valid Ku-band ranges (NR)		6a	16 20	3
range_numval_c	nr of valid C-band ranges		j1 j2 j3 sw	17 20	
range_numval	*alias of* range_numval_ka		sa		
range_numval	*alias of* range_numval_ku		other than sa		
range_numval_ku_nr	*alias of* range_numval_ku_adaptive		j3 sw		3

Notes:

1. A separate range measurement based on the MLE3 retracker is available for Jason-2 and -3, as well as for Sentinel-6, SWOT and TOPEX.

2. A separate range measurement based on the PLRM processing is available for Sentinel-3 and CryoSat-2.

3. The adaptive (for Jason-3 and SWOT) and numerical retracking (NR, for Sentinel-6) replace the conventional MLE retracking. It is more accurate and better takes into account the change of the instrument's point target response (PTR). For convenience an alias range_rms_ku_nr for range_rms_ku_adaptive is provided.

4. Standard deviation of S-band range for Envisat is available only until the loss of the S-band signal.

5. There can be 21 Sentinel-3 SAR mode measurements in one second.

3.4   Dry tropospheric correction and air tide

The dry tropospheric correction (the negative of the zenith hydrostatic delay, ZHD) accounts for the delay of the radar signal in the atmosphere, not counting the effect of water vapour. This effect is non-dispersive, i.e., it is the same on all frequencies, and is proportional to the

surface pressure [*Saastamoinen*, 1972]. The surface pressure, in turn, is determined by interpolation (in space and time) of model grids of surface (or sea level) pressure (see Notes). Most altimeter missions provide the ECMWF operational analysis models as baseline.

Generally, the temporal spacing of the model grids is 6 hours, while the spatial resolution varies. The 6-hourly interval between successive model grids hampers the capturing of 12-hourly and 24-hourly phenomena. Common 24-hourly traveling waves turn into standing waves, while 12-hourly variations are insufficiently described. These phenomena are considered S1 and S2 *air tides* [*Ponte and Ray*, 2002].

To remedy this problem an air tide correction is applied to the sea level pressure, by removing the air tide from the 6-hourly grids before spatio-temporal interpolation and then adding the air tide back for the time and location of the measurement. This correction is already applied to the ECMWF dry tropospheric correction on the Jason-2 GDRs; for all others it is corrected in the RADS processing.

Variable	name	units	sat	range	note
dry_tropo_ecmwf	ECWMF dry tropo corr	m	all but g1 gs tx pn	-2.4 -2.1	1
dry_tropo_ncep	NCEP dry tropo corr	m	all	-2.4 -2.1	2, 5
dry_tropo_era	ERA Interim dry tropo corr	m	all	-2.4 -2.1	3, 5
dry_tropo_era5	ERA5 dry tropo corr	m	3a 3b 6a j3 sw tx pn	-2.4 -2.1	4, 5
dry_tropo_airtide	air tide corr	m	c2 e1 j1		6
dry_tropo	*alias of* dry_tropo_era		g1 gs tx pn		
dry_tropo	*alias of* dry_tropo_ecmwf		other		

Notes:

1. The pressure fields on which this correction is based are from the ECMWF operational analysis runs. That means that numerous changes to the models and their resolution create an unstable reference for long-term studies. Please verify any of the ECMWF model results against the other models. Because of an unfortunate choice to use surface pressure fields, instead of sea level pressure fields, for this correction, coastal areas may be affected by "leaking" of the effect of higher terrain over land (thus lower pressure) into the sea and ocean (where there should be no terrain effect).

2. The NCEP reanalysis model used for this correction has *not* gone through any updates, so from that point of view the correction should be consistent over time. However, this older model also is less accurate and has a lower resolution ($2.5° \times 2.5°$) than the ECMWF analysis fields.

3. The ERA (ECMWF Reanalysis) Interim model provides an excellent long-term consistency. The data is distributed by ECMWF as Gaussian grids with an approximately uniform spacing of 79 km and 6-hourly temporal resolution[*Berrisford et al.*, 2011]. ECMWF discontinued this model in August 2019, so it is no longer added to the RADS data since then. All variables based on ERA Interim will thus be replaced by their equivalents based on ERA5.

4. The ERA5 (ECMWF Reanalysis v5) model is the latest ECMWF model aimed at climate-quality long-term consistency. The model grids input to RADS have a spatial resolution of $0.5° \times 0.5°$ and a temporal resolution of 1 hour. **Note that ERA5 model data is added with a delay of around 6 months.**

5. NCEP and ERA sea level pressure grids are interpolated and, over land and lakes, the pressure is then corrected for altitude based on a high-resolution terrain model, thus avoiding the coastal contamination seen in the ECMWF dry tropospheric correction.

6. The air tide correction to the dry tropospheric correction is provided for reference only. It is already applied to all variations of the dry tropospheric correction (ECMWF, NCEP, ERA interim, ERA5).

3.5   Wet tropospheric correction

The wet tropospheric correction (the negative of zenith wet delay, ZWD) accounts for the delay of the radar signal in the atmosphere due to the presence of water vapour. This effect is non-dispersive, i.e., it is the same on Ku-, S- and C-band frequencies, and it can be determined by integrating a function of water vapour density and temperature [e.g., *Askne and Nordius*, 1987], which to good approximation simplifies to

$$ZWD = IWV R_w (k_3/T_m + k_2')$$

where IWV is integrated water vapour, T_m is the mean temperature in the atmospheric column, and R_w, k_2' and k_3 are constants [*Bevis et al.*, 1994]. The mean temperature can further be approximated from model data of near-surface air temperature, T_s, by

$$T_m = 50.4 + 0.789 T_s$$

[*Mendes et al.*, 2000]. In this way, the 6-hourly models of integrated water vapour and near-surface temperature are interpolated in space and time and then converted to a wet tropospheric correction. Generally, the temporal spacing of the model grids is 6 hours, but since the power of the water vapour content at 12 and 24 hours is low, an air tide correction like in case of the pressure is not needed.

Because of the large spatial and temporal variability (much more so than pressure), most altimeter missions are equipped with passive microwave radiometers, collecting brightness temperatures of the ocean surface at two or three frequencies. Using the three frequencies, or two frequencies plus the radar altimeter backscatter measurement, a wet tropospheric correction (and some related variables) can be derived. However, the radiometer measurements are strongly affected by land in the measurement footprint (extending to a radius of 40 km in some cases), limiting its use in coastal regions, hence the existence of a radiometer land flag.

The radiometer wet tropospheric correction for ERS-1, ERS-2, and Envisat is based on the altimeter backscatter coefficient (before correction for atmospheric attenuation) and the radiometer brightness temperatures at 23.8 GHz and 36.5 GHz, using all the same neural network algorithm as was developed for Envisat [*Labroue and Obligis*, 2003]. For TOPEX/Poseidon, Jason-1 and -2, the radiometer wet tropospheric correction is derived from their respective 3-channel brightness temperatures using multi-layer parametric algorithms [*Keihm et al.*, 1995; *Dumont et al.*, 2001]. For GFO, the the 2-channel brightness temperatures are combined with the altimeter wind speed using a log-linear model [*Ruf et al.*, 1996]. See Sections 4.2 and 5.1 for information about corrections applied to the backscatter and brightness temperatures prior to evaluating the models.

Variable	name	units	sat	range	note
wet_tropo_rad	radiometer wet tropo corr	m	n1	-0.6 0.05	1
			pn tx	-0.6 -0.001	2
			e2	-0.6 0.0	3
			e1 g1 j1 j2 j3 sw	-0.6 0.0	
wet_tropo_ecmwf	ECMWF wet tropo corr	m	all but g1 gs	-0.6 0.0	4
wet_tropo_ncep	NCEP wet tropo corr	m	all	-0.6 0.0	5
wet_tropo_nvap	NASA NVAP wet tropo corr	m	gs	-0.6 0.0	6
wet_tropo_tovs_ssmi	TOVS/SSMI wet tropo corr	m	gs	-0.6 0.0	7
wet_tropo_tovs_ncep	TOVS/NCEP wet tropo corr	m	gs	-0.6 0.0	8
wet_tropo_era	ERA interim wet tropo corr	m	all	-0.6 0.0	9
wet_tropo_era5	ERA5 wet tropo corr	m	3a 3b 6a j3 sw tx pn	-0.6 0.0	10
wet_tropo	*alias of* wet_tropo_ecmwf		c2		11
wet_tropo	*alias of* wet_tropo_era		gs		11
wet_tropo	*alias of* wet_tropo_rad wet_tropo_era		g1		11
wet_tropo	*alias of* wet_tropo_rad wet_tropo_ecmwf		other		11

Notes:

1. Because of model bias and noise, allow positive values.

2. The TOPEX Microwave Radiometer (TMR) measurements values come from the TMR Replacement Product, version 1.0 (https://podaac.jpl.nasa.gov/dataset/TOPEX_L2_OST_TMR_Replacement). The upper limit of -0.001 m for the radiometer wet tropospheric correction is needed to exclude bogus zero values.

3. ERS-2 MWR is not available from 2009-05-04 to 2010-01-15.

4. The ECMWF correction is actually computed by integrating several layers of the atmosphere, rather than using the simplified form discussed above. The meteorological fields on which this correction is based are from the ECMWF operational analysis runs. That means that numerous changes to the models and their resolution create an unstable reference for long-term studies. Please verify any of the ECMWF model results against the other models.

5. NCEP reanalysis model used for this correction has *not* gone through any updates, so from that point of view the correction should be consistent over time. However, this older model also is less accurate and has a lower resolution (2.5°×2.5°) than the ECMWF analysis fields.

6. The NASA NVAP model is an old water vapour model used in the Geosat era.

7. TOVS and SSMI are separate radiometer constellations whose data were used to model the water vapour content globally.

8. This the result of a merger of the TOVS radiometer data with the NCEP water vapour and near-surface temperature models.

9. The ERA (ECMWF Reanalysis) Interim model provides an excellent long-term consistency. The data is distributed by ECMWF as Gaussian grids with an approximately uniform spacing of 79 km and 6-hourly temporal resolution[*Berrisford et al.*, 2011]. ECMWF discontinued this model in August 2019, so it is no longer added to the RADS data since then. All variables based on ERA Interim will thus be replaced by their equivalents based on ERA5.

10. The ERA5 (ECMWF Reanalysis v5) model is the latest ECMWF model aimed at climate-quality long-term consistency. The model grids input to RADS have a spatial resolution of $0.5° \times 0.5°$ and a temporal resolution of 1 hour. **Note that ERA5 model data is added with a delay of around 6 months.**

11. CryoSat-2 and Geosat have no radiometer, so the wet tropospheric correction is always based on models. For the other missions we may default to the model if the radiometer correction is not *at all* available on the product. This would be the case when the radiometer is *permanently* switched off, or off for a long time. The model will not be used during short outages.

3.6   Ionospheric correction

The radar signal is also delayed by ions and electrons in the upper layers of the atmosphere (the ionosphere). The delay is inversely proportional to the altimeter radar frequency, and otherwise proportional to the vertically integrated electron density, known as total electron content or TEC. This dispersive nature allows dual-frequency altimeters (TOPEX, Envisat, Jason-1 and -2) to directly determine the ionospheric path delay on either frequency. For single frequency altimeters we rely on TEC estimates from models based on other dual-frequency equipment (GPS, DORIS) or climatologies.

Variable	name	units	sat	range	note
iono_alt	dual-frequency iono corr	m	n1 j1 j2 j3 sw tx	-0.4 0.04	1
iono_alt_smooth	smoothed dual-freq iono cord	m	n1 j1 j2 j3 sw tx	-0.4 0.04	2
iono_bent	Bent iono corr	m	e1 e2	-0.4 0.04	3
iono_doris	DORIS iono corr	m	n1 pn	-0.4 0.04	4
iono_gim	JPL GIM iono corr	m	all but gs e1 pn	-0.4 0.04	5
iono_nic09	NIC09 iono corr	m	all	-0.4 0.04	6
iono_alt_mle3	dual-freq iono corr (MLE3)	m	6a j2 j3 sw tx	-0.4 0.04	7
iono_alt_smooth_mle3	smoothed d-f iono corr (MLE3)	m	j2 j3 sw tx	-0.4 0.04	7
iono_alt_plrm	dual-freq iono corr (PLRM)	m	3a 3b	-0.4 0.04	8
iono_alt_smooth_plrm	smoothed d-f iono corr (PLRM)	m	3a 3b	-0.4 0.04	8
iono_alt_adaptive	dual-freq iono corr (adap)	m	j3 sw	-0.4 0.04	9
iono_alt_smooth_adaptive	smoothed d-f iono corr (adap)	m	j3 sw	-0.4 0.04	9
iono_alt_nr	dual-freq iono corr (NR)	m	6a	-0.4 0.04	9
iono_alt_smooth_nr	smoothed d-f iono corr (NR)	m	6a	-0.4 0.04	9
iono	*alias of* iono_nic09		e1 gs		10
iono	*alias of* iono_gim iono_nic09		c2 e2 g1 sa pn		10
iono	*alias of* iono_alt_smooth		3a 3b 6a j1 j2 j3		
	iono_gim iono_nic09		n1 sw tx		10
iono_alt_nr	*alias of* iono_alt_adaptive		j3 sw		9
iono_alt_smooth_nr	*alias of* iono_alt_smooth_adaptive		j3 sw		9

Notes:

1. Positive correction values are allowed to account for noise in the altimeter dual-frequency ionospheric correction. The values for this correction have been adjusted from the original GDR products to account for relative C-band and S-band biases (Section 3.2).

2. Because of the relatively large noise in the dual-frequency ionospheric correction, iono_alt is smoothed along-track using a combination of a median filter and a Lanczos filter. For Jason-1 and -2, this replaces an earlier implementation of a box-car filter. For TOPEX, this variable was not available in the original product and was added in RADS.

3. The "ancient" Bent TEC climatology [*Llewellyn and Bent*, 1973] should no longer be used.

4. The TEC model based on DORIS featured for a while on TOPEX/Poseidon and Envisat altimeter products but was far behind the accuracy of the (similar in construct) GPS-derived GIM models.

5. JPL produces, based on the global constellation of GPS satellites and IGS GPS receivers, 2-hourly maps of TEC, known as the JPL GIM model [*Komjathy et al.*, 2000]. The models have a spatial resolution of $5° × 2.5°$ and start in August 1998.

6. The NIC09 climatology is based on 12 years of JPL GIM maps and can be extended as far back as the 1950s or extrapolated using predicted solar flux values [*Scharroo and Smith*, 2010]. This model is particularly useful for the period prior to August 1998 (before the availability of iono_gim).

7. A separate dual-frequency ionospheric based on the MLE3 retracker outputs is available for Jason-2 and -3, as well as for Sentinel-6, SWOT and TOPEX.

8. A separate dual-frequency correction based on the PLRM processing is available for Sentinel-3.

9. The adaptive (for Jason-3 and SWOT) and numerical retracking (for Sentinel-6) replace the conventional MLE retracking. Dual-frequency ionospheric corrections using these methods are available for these satellites. For convenience an alias iono_alt_nr for iono_alt_adaptive and an alias iono_alt_smooth_nr for iono_alt_smooth_adaptive are provided.

10. The alias iono will use either the smoothed dual-frequency ionospheric correction or one of the models in the order as given.

3.7 Atmospheric (inverse barometer) correction

The inverse barometer (IB) correction accounts for the suppression of sea level due to higher sea level pressure, and its rise during lower sea level pressure. When we assume a linear relation between pressure and suppression we talk about a "static" IB correction, and because the sea level goes down with increasing pressure, opposite to the way we think of a mercury barometer, we use the term "inverse". The simplest form of this correction is:

$$\text{IB} = C(p - p_0)$$

where C is -9.948 mm/mbar, p is the sea level pressure and p_0 is a reference pressure. Since the global ocean as a whole is incompressible, p_0 here stands for the global mean sea level pressure over oceans.

However, there are also dynamics involved in this. For example, an ocean basin cannot instantly be suppressed as a whole because of rapidly increasing regional pressure. Also wind can play a role as well. Hence, the static correction is too simplistic. A more accurate model includes wind and ocean dynamics and is hence called a dynamic atmospheric correction (DAC). RADS, AVISO, and other altimeter datasets include the dynamic atmospheric correction produced by CLS Space Oceanography Division using the MOG2D model from Legos [*Carrère and Lyard*, 2003; *Roblou et al.*, 2008] and distributed by AVISO, with support from CNES. A more recent update of the MOG2D correction files is based on forcing by the ERA Interim atmospheric models. Those have been made available for the period 1991 through 2015 [*Carrère et al.*, 2016].

Over inland waters, this correction should not be applied [*Crétaux and Birkett*, 2006].

Variable	name	units	sat	range	note
inv_bar_static	static inverse baro corr	m	all	-1 1	1
inv_bar_global	global mean inv baro corr	m	all	-1 1	2
inv_bar_mog2d	MOG2D/TUGO dynamic atmospheric corr	m	all	-1 1	3
inv_bar_mog2d_era	MOG2D/TUGO DAC from ERA-Int.	m	all	-1 1	4
inv_bar_mok2d	MOK2D dynamic atmospheric corr	m	all	-1 1	5
inv_bar_mog2d_mean	local mean of MOG2D	m	all	-1 1	6
dac	*alias of* inv_bar_mog2d_era inv_bar_mog2d		all		7
	inv_bar_mok2d				7
inv_bar	*alias of* dac		all		7

Notes:

1. This correction is the simplification explained above.

2. For reference the global mean pressure, converted to an IB correction, Cp_0, is provided.

3. The dynamic atmospheric correction model MOG2D (later replaced by TUGO) includes the ocean dynamic response to wind and pressure forcing. It also accounts for the aliasing of the air tides as discussed in Section 3.4. MOG2D also comes with two latencies: (a) a few days, and thus features on the IGDR-derived products, and (b) a few weeks, and thus features on the GDR-derived products. For fast-delivery products there is generally no MOG2D correction (so MOK2D will be used), but the MOG2D field will be filled in as soon as the MOG2D maps have been distributed.

4. The DAC based on forcing by the ECMWF ERA Interim atmospheric reanalysis model is available as inv_bar_mog2d_era. When choosing the detail DAC (either dac or inv_bar) this model is used for the years 1991 through 2015. After that inv_bar_mog2d or inv_bar_mok2d.

5. Since the MOG2D only start in 1992, we have created a "mock-up" version of MOG2D (a simple linear variant of inv_bar_static) to match the mean of MOG2D as to not disturb continuity of the DAC prior to 1992..

6. For reference, the local long-term mean of the MOG2D correction is provided. This is the interpolation of a static grid computed as the average of all MOG2D maps over the period 1993-2009.

7. When using the inv_bar or dac alias, inv_bar_mog2d_era is used when available (1991-2015), otherwise inv_bar_mog2d is used, or automatically defaulting to inv_bar_mok2d.

3.8   Solid earth and pole tide

The solid earth tide is the variation of the elevation of the crust of the earth surface as a result of the attraction by the sun and moon (other planets are generally ignored as their influence is at least an order of magnitude smaller). As per geodetic convention the "permanent tide" (the mean tide resulting from the mere presence of the sun and moon) is excluded from the solid earth tide but is included in the geoid.

The RADS implementation of the Cartwright-Taylor-Edden solid earth tide model includes 386 second order waves and 99 third order waves [*Cartwright and Taylor*, 1971; *Cartwright and Edden*, 1973].

The pole tide is the vertical deformation of the earth crust as a result of polar motion. We can visualise this as the ellipsoidal shape of the earth being moved as the rotation axis of the earth moves away or closer to the mean pole [*Munk and MacDonald*, 1960]. We use the

IERS(EOP)05C04 earth orientation parameters and their predictions. The motion of the mean pole, describing the effect of global isostatic adjustment (GIA) is represented by a linear motion, as suggested by *Wahr et al.* [2015] following the work of *Argus and Gross* [2004]. The implicit effect on pole tide is further discussed by *Desai et al.* [2015].

Two Love numbers multiply the results of this simple equilibrium model: $(1 + k_2) = 1.302$ for the combination of solid earth and oceans, and $h_2 = 0.609$ for the solid earth only (over land and lakes) [*Wahr*, 1985].

Variable	name	units	sat	range	note
tide_solid	solid earth tide	m	all	-1 1	
tide_pole	pole tide	m	all	-0.1 0.1	

3.9 Ocean and load tide

The (pure) ocean tide is the variation of the height of the water column as a result of luni-solar attraction. Since this is measured relative to a fixed point on the solid earth (like the sea floor), the ocean tide compares directly to tide gauge measurements. The load tide is the effect of the tides weighing on the elastic earth. In general, when the ocean tide goes up, the sea floor is going down, hence reducing the sum of the two, the geocentric ocean tide. Consequently, in order to detide the measurement of the water surface from altimetry, both the ocean tide (tide_ocean) and the load tide (tide_load) need to be subtracted over ocean surfaces, while over lakes only the load tide is subtracted.

Although some altimeter products provide the geocentric ocean tide, we have chosen to keep ocean and load tide separate, for two reasons: (1) it makes it easier to differentiate tides over land/lakes and ocean, and (2) it makes it easier to add regional tides which are generally expressed as pure ocean tides.

Tides are expressed as the sum of a (large) number of *waves* with different frequencies, each combinations of the frequencies associated with the rotation and progression of the earth, sun and moon. A select portion of those waves are expressed as grids of amplitude and phase, which can be interpolated in space and evaluated at the time of the altimeter measurement. Then, by a process called *admittance*, the amplitude and phase of a number of minor tides are inferred.

Tide models generally only include the diurnal and semi-diurnal waves (those around a period of 12 and 24 hours). On top of that there are secondary and tertiary waves with periods of a week or longer. Most of these waves can be expressed by a simple latitude and time dependent equilibrium model (the long-period equilibrium tide). The FES ocean tide models also include the non-equilibrium component of the monthly, fortnightly, tri-monthly, and weekly tides.

Although the FES and GOT models are global, they are limited in scope. Over land, the ocean tide is not defined and will be set to the NaN value. In some coastal regions, where the models may likely not be defined, the ocean tide value is set to NaN as well.

For a very elaborate and thorough accuracy assessment of most of these tide models, we highly recommend reading the work by *Stammer et al.* [2014].

Variable	name	units	sat	range	note
tide_ocean_fes04	FES2004 ocean tide	m	all	-5 5	1
tide_load_fes04	FES2004 load tide	m	all	-0.5 0.5	1
tide_ocean_webtide	WebTide ocean tide	m	all	-5 5	2
tide_ocean_got48	GOT4.8 ocean tide	m	all	-5 5	3
tide_load_got48	GOT4.8 load tide	m	all	-0.5 0.5	3
tide_ocean_got410	GOT4.10c ocean tide	m	all	-5 5	4
tide_load_got410	GOT4.10c load tide	m	all	-0.5 0.5	4
tide_ocean_fes14	FES2014b ocean tide	m	all	-5 5	5
tide_load_fes14	FES2014a load tide	m	all	-0.5 0.5	5
tide_equil	long-period equilib. tide	m	all	-1 1	6
tide_non_equil	long-period non-equil. tide	m	all	-1 1	7
tide_ocean	*alias of* tide_ocean_fes14		all		
tide_load	*alias of* tide_load_fes14		all		

Notes:

1. The Finite Element Solution (FES2004) includes 9 short-period waves (Q1, O1, K1, P1, 2N2, N2, M2, K2, and S2) plus 24 additional short-period waves determined by admittance, and 4 long-period waves (Mf, Mm, Mtm and MSqm) [*Lyard et al.*, 2006]. Long-period equilibrium tides (not yet included in FES2004) are added to these.

2. WebTide is a collection of regional tide models along the Canadian coast, made available on the web by the Bedford Institute of Oceanography http://www.bio.gc.ca/research-recherche/WebTide-MareeWeb/webtide-eng.htm. In RADS, a single value is presented in tide_ocean_webtide, determined from (in order of decreasing preference) the regional models for: Scotia/Fundy/Maine, Northeast Pacific, Arctic, Hudson Bay. Each of these models has a very limited amount of constituents, does not include admittance to infer others, and also does not include any long-period tides (equilibrium or non-equilibrium).

3. The Goddard Ocean Tide model GOT 4.8 includes 10 short-period waves (K1, O1, P1, Q1, S1, K2, M2, N2, S2, and M4) plus 17 additional short-period waves determined by admittance [*Ray et al.*, 2011].

4. The Goddard Ocean Tide model GOT4.10c differs from GOT4.8 in two ways. First, GOT4.10c is based only on Jason data, whereas 4.8 was from only TOPEX data. Second, it includes an adjustment for the geocenter. (Hence the 'c' in the name.) The processing for 4.8 and 4.10 was largely identical; one exception involved an improvement to P1 alone. GOT4.10c is an update of *Ray* [2013].

5. FES2014 (Finite Element Solution 2014) takes advantage of longer altimeter time series, improved modelling, and data assimilation techniques, and more accurate and higher resolution ocean bathymetry. A new global finite element grid (with approx. 1.5 million nodes) was used to create a 'free' solution (independent of in situ and remote-sensing data) that has more than twice the accuracy of the FES2004 version. The 'free' solution was assimilated with long-term altimetry data from TOPEX/POSEIDON, Jason-1, Jason-2, ERS-1, ERS-2, and ENVISAT. The FES2014 solution shows particular improvement in coastal and shelf regions, as well as in overall open ocean statistics, particularly due to a higher grid resolution (1/16°). The model is also extended into the coast to improve the data coverage. As with other FES models tide_ocean_fes14 includes long-period non-equilibrium tides; specifically: Mf, Mm, Mtm, MSf, MSqm, Sa, and Ssa. This model is now the default tide model.

6. The equilibrium ocean tide includes 15 tidal spectrum lines from the Cartwright-Tayler-Edden tables [*Cartwright and Taylor*, 1971; *Cartwright and Edden*, 1973] plus an additional 123 second and third order waves [*Tamura*, 1987].

7. The four long-period non-equlibrium ocean tidal components (Mm, Mf, MSf, Mtm, and MSqm) from the FES2004 model are represented in tide_non_equil. The equilibrium parts of those have been removed to avoid double accounting.

3.10   Internal tides

In places where ocean topography changes significantly, the predominant barotropic tides are converted to baroclinic tides, which then also produce an expression in the sea surface with much smaller wavelengths than the normal solar-lunar ocean tides. Altimetry observes those components that are phase locked with the astronomical tide forcing [*Ray and Zaron*, 2016].

Zaron [2019] produced a near-global model for the internal tides with the components K1, O1, M2, S2 plus the annual modulates of M2, named MA2 and MB2. In RADS, as per recommendation of the author, only the first four components are used in the development of the internal tide predection.

Variable	name	units	sat	range	note
tide_internal	HRET v8.1 internal tide	m	3a 3b 6a c2 j1 j2 j3 sa tx pn	1	

Note

1. The high-resolution emperical tide (HRET) v8.1 [*Zaron*, 2019] is **not** incorporated in the ocean tide, and is **not**, by default, accounted for in the sea level anomaly sla.

3.11   Sea state bias

Sea state bias (SSB) is the term used for any altimetric range offset as a function of the sea state (wave height, wind speed, wave age, swell). In fact, there are three components to the sea state bias:

Electromagnetic (EM) bias is the tendency of a radar to measure towards the wave troughs since they are better reflectors than the wave peaks.

Skewness bias comes from the fact that the sea surface has a skewed height distribution. While the altimeter measures the median height of the surface in the footprint, what we want to measure is the mean height, which is lower.

Tracker bias is the any error in the waveform tracker that is a function of the sea state, which may be either instrumental or algorithmic.

Because of the instrumental part of sea state bias, every altimeter, in principle, requires a different sea state bias correction model. But also when a new tracker algorithm is implemented, the sea state bias changes. This is one of the reasons for the wide proliferation of SSB models.

In the earlier days of altimetry the sea state bias was generally considered as a simple fraction, around –3.5%, of significant wave height [*Chelton*, 1994]. Then *Gaspar et al.* [1994] brought a major improvement in SSB modelling by expressing SSB as a polynomial function of SWH

and wind speed, recognising that not only the wave height, but also the shape of the waves (altered by wind) has influence on the altimeter range bias. But this approach still exhibits some limitations, in that it imposes the type of variations that are allowed as a result of changes in SWH or wind speed. Currently, SSB models tend to be non-parametric, generally expressed in the form of a grid with SWH and wind speed as coordinates [e.g., *Gaspar and Florens*, 1998]. But several more complex multi-dimensional models are currently under development [e.g., *Feng et al.*, 2010; *Tran et al.*, 2010].

Variable	name	units	sat	range	note
ssb_bm3	parametric sea state bias	m	e1 e2 g1 gs pn	-1 1	1
ssb_cls	CLS non-param. SSB	m	3a 3b 6a c2 j1 j2 j3 n1 sw	-1 1	2
ssb_cls_mle3	CLS non-param. SSB (MLE3)	m	6a j2 j3 sw	-1 1	3
ssb_cls_plrm	CLS non-param. SSB (PLRM)	m	3a 3b c2	-1 1	4
ssb_cls_adaptive	CLS non-param. SSB (adap.)	m	j3 sw	-1 1	8
ssb_cls_3d	CLS 3D non-param. SSB	m	j3 sw	-1 1	7
ssb_cls_3d_adaptive	CLS 3D non-param. SSB (adap.)	m	j3	-1 1	8
ssb_cls_nr	CLS non-param. SSB (NR)	m	6a	-1 1	8
ssb_cls_c	CLS non-param. SSB (C-band)	m	3a 3b 6a j1 j2 j3 sw	-1 1	2
ssb_cls_c_adaptive	CLS non-param. SSB (C-band, adap.)	m	j3 sw	-1 1	8
ssb_cls_c_nr	CLS non-param. SSB (C-band, NR)	m	6a	-1 1	8
ssb_hyb	NOAA hybrid sea state bias	m	g1 gs n1 sa	-1 1	5
ssb_tran2012	Tran et al. 2012 non-param. SSB	m	j1 j2 sw	-1 1	6
ssb_tran2019	Tran et al. 2019 non-param. SSB	m	sa	-1 1	7
ssb_tran2019_3d	Tran et al. 2019 3D non-param. SSB	m	sa	-1 1	7
ssb_tx	TOPEX GDR-F SSB	m	tx	-1 1	9
ssb_tx_mle3	TOPEX GDR-F SSB (MLE3)	m	tx	-1 1	9
ssb_tx_c	TOPEX GDR-F SSB (C-band)	m	tx	-1 1	9
ssb	*alias of* ssb_bm3		e1 e2 pn		
ssb	*alias of* ssb_cls		j1 j2 j3 n1 sw		
ssb	*alias of* ssb_hyb		c2 g1 gs sa		
ssb_cls_nr	*alias of* ssb_cls_adaptive		j3 sw		8
ssb_cls_c_nr	*alias of* ssb_cls_c_adaptive		j3 sw		8

Notes:

1. One-, three- or four-term polynomials of SWH and wind speed [*Gaspar et al.*, 1994].

2. Non-parametric sea state bias models for Ku-band and C-band by CLS [*Gaspar et al.*, 2002; *Labroue et al.*, 2004].

3. A separate sea state bias correction based on and for the correction of the MLE3 retracker outputs is available for Jason-2 and -3, as well as for Sentinel-6 and SWOT.

4. A separate sea state bias correction based on and for the correction of the PLRM processing outputs is available for Sentinel-3 and CryoSat-2.

5. Hybrid (mix between parametric and non-parametric techniques) sea state bias models produced at NOAA [*Scharroo and Lillibridge*, 2005].

6. The non-parametric SSB model developed by *Tran et al.* [2012] is part of the GDR-E and GDR-F standards.

7. [*Tran et al.*, 2021] is a reference for a number of 2D (ssb_tran_2019) and 3D (ssb_tran_2019_3d) sea state bias models.

8. The adaptive (for Jason-3 and SWOT) and numerical retracking (for Sentinel-6) replace the conventional MLE retracking. Sea state bias values using SWH and wind speed from

those retrackers are available for these satellites. For convenience an alias ssb_cls_nr for ssb_cls_adaptive and an alias ssb_cls_c_nr for ssb_cls_c_adaptive are provided.

9. For the TOPEX reprocessed data *Putnam Shileah* [2021] developed specific models for Side A and Side B, providing the correction for Ku-band data with MLE4 (ssb_tx) or MLE3 (ssb_tx_mle3) retrackers or for C-band data (ssb_tx_c).

3.12   Mean sea surface and geoid

The sea level anomaly (SLA) is expressed as the difference of the instantaneous tide-corrected sea surface with respect to a well-established mean. Over the years several (more or less) global mean sea surface models have been developed from the compilation of satellite altimeter (and sometimes gravity) data. Generally, the more altimeter data collected, the more precise the model. But also the resolution of the model counts. Each model has been referenced to the TOPEX reference ellipsoid, just as the satellite orbits (Section 2.3).

Another reference surface is the geoid (the theoretical mean sea surface in absence of ocean currents, wind, etc.). Geoid models are generally made from satellite tracking data (for the longer wave lengths), GRACE and/or GOCE (for the medium wave lengths), and altimetry and in-situ gravimetry (for the shorter wave lengths).

Variable	name	units	sat	range	note
mss_cnescls11	CNES-CLS11 mean sea surface	m	e1 e2 g1 gs	-200 200	1
mss_cnescls15	CNES-CLS15 mean sea surface	m	all but e1 e2 g1 gs n1	-200 200	2
mss_cnescls22	CNES-CLS22 mean sea surface	m	(none yet)	-200 200	3
mss_dtu13	DTU13 mean sea surface	m	e1 e2 g1 gs n1	-200 200	4
mss_dtu15	DTU15 mean sea surface	m	all	-200 200	5
mss_dtu18	DTU18 mean sea surface	m	all but e1 e2 g1 gs n1	-200 200	6
mss_dtu21	DTU21 mean sea surface	m	all but e1 e2 g1 gs n1	-200 200	6
mss_comb15	Comb. SIO/CNES-CLS15/DTU15	m	all but e1 e2 g1 gs n1	-200 200	7
geoid_egm2008	EGM2008 geoid	m	all	-200 200	8
geoid_eigen6	EIGEN-6C3stat geoid	m	all	-200 200	9
mss	*alias of* mss_dtu15		all		
geoid	*alias of* geoid_egm2008		all		

Notes:

1. Iteration of mean sea surface models at CNES/CLS from 2011, based on altimeter data from 1993 to 1999 [*Schaeffer et al.*, 2012]. **This variable is deprecated and slated for removal from the RADS data base.**

2. Latest iteration of mean sea surface models at CNES/CLS from 2015, based on altimeter data from 1993 to 2012 [*Schaeffer et al.*, 2012].

3. The CNES/CLS mean sea surface model from 2022 covers altimeter data spread over 20 years, including CryoSat-2 and SARAL/AltiKa data [*Schaeffer et al.*, 2023]. It is not yet introduced in RADS, but may be in the near future to replace some of the older MSS models.

4. The DTU13MSS is an older release of the global high-resolution mean sea surface from DTU Space, which includes two major advances over DTU10MSS. First, the time series have been extended to 20 years from 17 years. Second, the DTU13MSS ingests Cryosat-2 SAR lead data in order to map the high latitude parts of the Arctic Ocean. In high-latitude

regions a combination of joint ERS-1/ERS-2/ENVISAT and Cryosat-2 altimetry have been used. Also, the Jason-1 geodetic mission has been used for the DTU13MSS [*Andersen et al.*, 2013]. **This variable is deprecated and slated for removal from the RADS data base.**

5. The DTU15MSS is a later version of the global high-resolution mean sea surface derived by DTU Space from satellite altimetry. The main improvement over DTU13 is the inclusion of four years of CryoSat-2 data, with a new treatment of orbit errors and ice classification [*Stenseng et al.*, 2015]. This is the **default mean sea surface model** and is used as reference for the sea level anomaly variable (sla).

6. The DTU18MSS [*Andersen et al.*, 2018] and DTU21MSS [*Andersen et al.*, 2023] are two recent iterations of the global high-resolution mean sea surface derived by DTU Space from satellite altimetry.

7. The combined SIO/CNES-CLS15/DTU15 mean sea surface model is a collaborate merge of all the best bits of three different mean sea surface models [*AVISO*, 2021].

8. Combined geoid and mean sea surface solution from the US Defence Mapping Agency [*Pavlis et al.*, 2012]. This is the **default geoid model**.

9. The EIGEN-6C3stat geoid model has been generated in preparation for the final release of EIGEN-6C4. It was computed from a combination of LAGEOS, GRACE, and GOCE data, augmented with DTU13 surface gravity data to degree and order 1949 (corresponding to approximately 10 km spatial resolution). [*Förste et al.*, 2013; *Shako et al.*, 2014].

Chapter *4*

Wind speed and wave height variables

4.1 Significant wave height

The significant wave height (SWH) is generally defined as the mean wave height (peak to trough) of the highest one-third of the ocean waves. Another commonly used definition is four times the standard deviation of the elevation of the sea surface in the radar footprint.

In MLE3 and MLE4 retrackers, the SWH is determined from the rate of increase of returned power of the radar altimeter pulse (the waveform slope) and requires no further correction other than some instrument parameters. There is one complexity in this, and that is that SWH is defined as follows:

$$\text{SWH}^2 = \alpha^2(\sigma_c^2 - \sigma_p^2)$$

where σ_c is a measure of the waveform slope and σ_p is an instrument parameter, and α is a constant. Because of noise in the measurement of σ_c and a possible bias in σ_p, SWH^2 could become negative. In most GDR products, SWH is then set to zero, which creates a wrongly truncated measurement, and makes it difficult to correct for any biases in SWH the measurement (which would raise the zero SWH above zero). Where we can, however, in RADS, this case is tackled by writing out the negative of the square root of the absolute value of the argument instead. Hence:

$$\text{SWH} = -\alpha\sqrt{\sigma_p^2 - \sigma_c^2} \quad \text{when} \quad \sigma_c < \sigma_p$$

$$\text{SWH} = \alpha\sqrt{\sigma_c^2 - \sigma_p^2} \quad \text{when} \quad \sigma_c \geq \sigma_p$$

(See Note 1 below).

Fortunately, for SAR altimeters, *i.e.* for Sentinel-3, Sentinel-6, and CryoSat-2, the SWH is a direct output of the retracking, so the complication with σ_c is avoided. This is also the case for the numerical and adaptive retrackers used for the low-resolution data of Jason-3 and Sentinel-6.

The 1-Hz standard deviation of SWH is determined from the individual 10-, 20-, or 40-Hz elementary measurements. Note that this is the standard deviation of the elementary measurements (denominator is $(n-1)$), not an estimate of the error of SWH.

For comparison with the altimeter-derived significant wave height, RADS also supplies some model outputs (*e.g.*, swh_mfwam and swh_era5).

Variable	name	units	sat	range	note
swh_ka	Ka-band significant wave height	m	sa	0 8	
swh_ku	Ku-band significant wave height	m	c2 n1	-0.5 8	1
			other	0 8	
swh_ku_mle3	Ku-band significant wave height (MLE3)	m	6a j2 j3 sw tx	0 8	2
swh_ku_plrm	Ku-band significant wave height (PLRM)	m	3a 3b c2	0 8	3
swh_ku_adaptive	Ku-band significant wave height (adap.)	m	j3 sw	0 8	4
swh_ku_nr	Ku-band significant wave height (NR)	m	6a	0 8	4
swh_c	C-band significant wave height	m	j1 j2 j3 sw tx	0 8	
swh_s	S-band significant wave height	m	n1	-0.5 8	1,5
swh_ww3	WAVEWATCH3 model SWH	m	c2 j2 j3 sa		6
swh_mfwam	MFWAM model significant wave height	m	3a 3b 6a j3 sw tx pn		7
swh_era5	ERA5 model significant wave height	m	3a 3b 6a j3 sw tx pn		8
swh	*alias of* swh_ka		sa		
swh	*alias of* swh_ku		other		
swh_ku_nr	*alias of* swh_ku_adaptive		j3 sw		4
swh_rms_ka	std dev of Ku-band SWH	m	sa	0 2.1	
swh_rms_ku	std dev of Ku-band SWH	m	g1	0 0.5	
			j1 j2 j3 sw tx	0 1.5	
			other	0 2.1	
swh_rms_ku_mle3	std dev of Ku-band SWH (MLE3)	m	6a j2 j3 sw tx	0 1.5	2
swh_rms_ku_plrm	std dev of Ku-band SWH (PLRM)	m	3a 3b c2	0 1.5	3
swh_rms_ku_adaptive	std dev of Ku-band SWH (adap.)	m	j3 sw	0 1.5	4
swh_rms_ku_nr	std dev of Ku-band SWH (NR)	m	6a	0 1.5	4
swh_rms_c	std dev of C-band SWH	m	3a 3b 6a j1 j2 j3 sw tx	0 2.1	
swh_rms_s	std dev of S-band SWH	m	n1	0 2.1	5
swh_rms	*alias of* swh_rms_ka		sa		
swh_rms	*alias of* swh_rms_ku		other		
swh_rms_ku_nr	*alias of* swh_rms_ku_adaptive		j3 sw		4

Notes:

1. The SWH of Envisat and CryoSat will be set to a negative value when $\sigma_c < \sigma_p$. For other missions, the value is set to 0.

2. A separate significant wave height measurement based on the MLE3 retracker is available for Jason-2 and -3, as well as for Sentinel-6, SWOT and TOPEX.

3. A separate significant wave height measurement based on the PLRM processing is available for Sentinel-3 and CryoSat-2.

4. The adaptive (for Jason-3 and SWOT) and numerical retracking (for Sentinel-6) replace the conventional MLE retracking. SWH measurements from those retrackers are available for these satellites. For convenience an alias swh_ku_nr for swh_ku_adaptive and an alias swh_rms_ku_nr for swh_rms_ku_adaptive are provided.

5. S-band SWH for Envisat is only until the loss of the S-band signal.

6. The SWH in this field is based on wave hindcasts done by NOAA using the WAVE-WATCH III model [*Tolman*, 2009] and GFS analysis winds [*Chawla et al.*, 2011]. The hindcasts cover the entire globe and are carried out in monthly installments, so they are only available on delay-time data in RADS. The original resolution of these model grids is 1° by 1° by 6 hours. For other WAVEWATCH III fields see Section 4.4. **This variable is deprecated and slated for removal from the RADS data base.**

7. Météo-France determines SWH from the WAM model (and other ocean parameters) every 6 hours with a spatial resolution of $1° \times 1°$. The spatio-temporally interpolated data are provided here.

8. The ERA5 (ECMWF Reanalysis v5) model is the latest ECMWF model aimed at climate-quality long-term consistency. The model grids input to RADS have a spatial resolution of $0.5° \times 0.5°$ and a temporal resolution of 1 hour. **Note that ERA5 model data is added with a delay of around 6 months.**

4.2   Altimeter backscatter coefficient

The backscatter coefficient is derived from the total returned power of the radar altimeter pulse. After correction for losses due to water vapour in the atmosphere, it identifies the small scale ripples on the sea surfaces, and hence becomes a measure for wind speed (Section 4.3).

The correction for atmospheric losses is generally determined from the radiometer measurements. In case the brightness temperatures were corrected with respect to the GDR values (Section 5.1), so is the wet tropospheric correction, the atmospheric correction to the backscatter and the backscatter coefficient itself.

The 1-Hz standard deviation of backscatter coefficient is determined from the individual 10-, 20- or 40-Hz elementary measurements. Note that this is the standard deviation of the elementary measurements (denominator is $(n-1)$), not an estimate of the error of the backscatter coefficient.

Variable	name	units	sat	range	note
sig0_ka	Ka-band backscatter coefficient	dB	sa	6 27	
sig0_ku	Ku-band backscatter coefficient	dB	other than sa	6 27	1-5
sig0_ku_mle3	Ku-band backscatter coefficient (MLE3)	dB	6a j2 j3 sw tx	6 27	6
sig0_ku_plrm	Ku-band backscatter coefficient (PLRM)	m	3a 3b c2	6 27	7
sig0_ku_adaptive	Ku-band backscatter coefficient (adap.)	dB	j3 sw	6 27	8
sig0_ku_nr	Ku-band backscatter coefficient (NR)	dB	6a	6 27	8
sig0_c	C-band backscatter coefficient	dB	j1 j2 j3 sw tx	6 27	3-5
sig0_s	S-band backscatter coefficient	dB	n1	6 27	9
sig0	*alias of* sig0_ka		sa		
sig0	*alias of* sig0_ku		other		
sig0_ku_nr	*alias of* sig0_ku_adaptive		j3 sw tx		8
sig0_rms_ka	std dev of Ka-band SWH	dB	sa	0 1	
sig0_rms_ku	std dev of Ku-band SWH	dB	other than sa	0 1	
sig0_rms_ku_mle3	std dev of Ku-band SWH (MLE3)	dB	6a j2 j3 sw tx	0 1	6
sig0_rms_ku_plrm	std dev of Ku-band SWH (PLRM)	dB	3a 3b c2	0 1	7
sig0_rms_ku_adaptive	std dev of Ku-band SWH (adap.)	dB	j3 sw	0 1	8
sig0_rms_ku_nr	std dev of Ku-band SWH (NR)	dB	6a	0 1	8
sig0_rms_c	std dev of C-band SWH	dB	j1 j2 j3 sw tx		
sig0_rms_s	std dev of S-band SWH	dB	n1		9
sig0_rms	*alias of* sig0_rms_ka		sa		
sig0_rms	*alias of* sig0_rms_ku		other		
sig0_rms_ku_nr	*alias of* sig0_rms_ku_adaptive		j3 sw		8

Notes:

1. The ERS-1 backscatter coefficient is corrected for varying biases due to the attitude control. Between 0 and 0.35 dB was added.

2. The GFO backscatter is corrected for a few deficiencies in lookup tables, adding 0.37 dB before 6 Dec 2000 and between 7 and 9 March 2001.

3. The Jason-1 Ku- and C-band backscatter are aligned with TOPEX values by subtracting 2.40 and 0.725 dB, respectively. For the time being, the same biases are applied to Jason-2. However, wind speed values are not adjusted.

4. The Jason-2 Ku- and C-band backscatter are reduced in noise based on a correlation with off-nadir angle [*Quartly*, 2009]. In addition, biases of 2.40 and 0.725 dB have been removed from the Ku- and C-band backscatter, respectively.

5. The Jason-3 Ku- and C-band backscatter are adjusted the same way as Jason-2.

6. A separate backscatter coefficient based on the MLE3 retracker is available for Jason-2 and -3, as well as for Sentinel-6, SWOT and TOPEX.

7. A separate backscatter coefficient based on the PLRM processing is available for Sentinel-3 and CryoSat-2.

8. The adaptive (for Jason-3 and SWOT) and numerical retracking (for Sentinel-6) replace the conventional MLE retracking. Backscatter coefficients from those retrackers are available for these satellites. For convenience an alias sig0_ku_nr for sig0_ku_adaptive and an alias sig0_rms_ku_nr for sig0_rms_ku_adaptive are provided.

9. S-band backscatter for Envisat is only until the loss of the S-band signal.

4.3 Wind speed

Wind speed can be derived from the altimeter backscatter coefficient (Section 4.2). The larger the backscatter, the lower the wind speed. Several models have been developed to map this relationship, some depending merely on backscatter, some also taking into account significant wave height. Which models are applied to which satellites is shown in the notes below.

Three-channel radiometers provide the opportunity to estimate wind speed. In essences this is the reverse side of the fact that one of those channels can be replaced with the altimeter wind speed to obtain the wet tropospheric correction. This variable is available for all missions with 3-channel radiometers.

Atmospheric models, like those at ECMWF also provide wind speed and wind directions, or their vectorial components pointing north and east. Those model values are provided for some missions as well.

Variable	name	units	sat	range	note
wind_speed_alt	altimeter wind speed	m/s	all	-1 30	1-5
wind_speed_alt_mle3	altimeter wind speed (MLE3)	dB	6a j2 j3 sw tx	6 27	6
wind_speed_alt_plrm	altimeter wind speed (PLRM)	m	3a 3b c2	6 27	7
wind_speed_alt_adaptive	altimeter wind speed (adap.)	dB	j3 sw	6 27	8
wind_speed_alt_nr	altimeter wind speed (NR)	dB	6a	6 27	8
wind_speed_rad	radiometer wind speed	m/s	6a j1 j2 j3 sw tx pn	0 30	9
wind_speed_ecmwf_u	ECMWF model wind speed (U)	m/s	e2 j1 j2 j3 n1 sa sw		10
wind_speed_ecmwf_v	ECMWF model wind speed (V)	m/s	e2 j1 j2 j3 n1 sa sw		10
wind_speed_ecmwf	ECMWF model wind speed	m/s	e2 j1 j2 j3 n1 sa sw		10
wind_speed_era5_u	ERA5 model wind speed (U)	m/s	3a 3b 6a j3 sw tx pn		11
wind_speed_era5_v	ERA5 model wind speed (V)	m/s	3a 3b 6a j3 sw tx pn		11
wind_speed_era5	ERA5 model wind speed	m/s	3a 3b 6a j3 sw tx pn		11
wind_speed	*alias of* wind_speed_alt		all		
wind_speed_alt_nr	*alias of* wind_speed_alt_adaptive		j3 sw		8

Notes:

1. For Geosat, GFO, ERS-1 and ERS-2, the wind speed is based on the Modified Chelton-Wentz (MCW) algorithm [*Witter and Chelton*, 1991]. In case of GFO 0.63 dB was subtracted from the backscatter coefficient before feeding it into the MCW algorithm.

2. The CryoSat and Envisat wind speed is based on the ECMWF 1-parameter algorithm tailored to Envisat [*Abdalla*, 2007].

3. The Ka-band altimeter of SARAL required a new 1-parameter algorithm, similar to Envisat's, again matching ECWMF wind fields [*Lillibridge et al.*, 2014].

4. The TOPEX/Poseidon wind speed is based on the 2-parameter model by *Gourrion et al.* [2002].

5. For Jason-1 and Jason-2, a variant of the 2-parameter model by *Gourrion et al.* [2002] tailored to Jason-1 is used to derive wind speed [*Collard*, 2005].

6. A separate wind speed based on the MLE3 retracker outputs is available for Jason-2 and -3, as well as for Sentinel-6, SWOT and TOPEX.

7. A separate wind speed based on the PLRM processing results is available for Sentinel-3 and CryoSat-2.

8. The adaptive (for Jason-3 and SWOT) and numerical retracking (for Sentinel-6) replace the conventional MLE retracking. Wind speed based on the outputs of those retrackers are available for these satellites. For convenience an alias wind_speed_alt_nr for wind_speed_alt_adaptive is provided.

9. The 3- and 6-channel radiometers provide a wind speed estimate based on radiometer measurements only.

10. The U (towards east) and V (towards north) components of the wind speed according to ECMWF analysis model data are stored on the RADS data. The absolute magnitude (wind_speed_ecmwf) can be computed on-the-fly.

11. The U (towards east) and V (towards north) components of the wind speed according to ECMWF Reanalysis v5 model data are stored on the RADS data. The absolute magnitude (wind_speed_era5) can be computed on-the-fly.

4.4   Other wave model data

For calibration and validation purposes, and to support further studies that include wind and wave processes (like swell and their effect on sea state bias) a number of variables from the Météo-France WAM model runs have been included. The original resolution of the model grids is 5 arcmin by 5 arcmin by 3 hours.

Variable	name	units	sat	range	note
swh_mfwam	significant wave height	m	3a 3b 6a j3 sw tx pn		
mean_wave_period	t02 mean wave period	s	3a 3b 6a j3 sa sw tx pn		
mean_wave_direction	mean dir. of sea surface wave	deg	3a 3b 6a j3 sa sw tx pn		
significant_swell_wave_height	significant swell wave height	m	3a 3b 6a		
mean_swellwave_period	mean swell wave period	s	3a 3b 6a		
mean_swell_wave_direction	mean direction of swell wave	deg	3a 3b 6a		

Chapter *5*

Radiometer variables

5.1   Radiometer brightness temperatures

5.2   Water vapour content

5.3   Liquid water content

Variables for data editing

6.1 Engineering and geophysical flags

The engineering and geophysical flags are historically a number of bits in a 2-byte integer number that describe either instrument settings, type of surface overflow, or warnings about the quality of the data. In RADS4 there are a number of *aliases* to help pick out single bits from this word. The editing, however, is currently still determined by the limits set on the flag word, where the lower limits indicates which bits of the flag word *should not* be set, and the upper limits indicates the bits of the flag word that *should* be set. In other words, a record will be rejected if either:

- flags AND flags_low is not equal to 0.
- flags AND flags_high is not equal to flags_high.

where flags_low and flags_high are the lower and higher limit of flags specified, and AND is the logical bitwise AND operator.

In a future version of the data base the flag word flags will be phased out and only the more elementary flag variables that are now defined as aliases will be available.

Variable	name	units	sat	range	note
flags	flag word		3a 3b	65448 0	1
			c2	32 0	
			6a e1 e2 j1 j2	65512 0	
			j3	65384 0	1
			g1	65384 0	
			gs	51176 0	
			n1	36712 0	
			pn	48 0	
			sw	65384 0	1
			tx	16360 0	
	alias of flags				

Notes:

1. This is a temporary value, where the radiometer land flag is not considered as an edit criterion.

The individual bits of the flag word flags are described in the following table. Note that the limits on these alias are not actually set at this time, but they are a transposition of the editing ranges for each individual altimeter as indicated in the table above. In general, 0 means no or OK, 1 means yes or bad.

Variable	name	values	sat	note
flag_alt_oper_mode	bit 0: hardware/software status	0 = nominal, 1 = bad	pn tx	
	bit 0: altimeter operating mode	0 = Side A, 1 = Side B	j1 j2 j3 n1 sw	
	bit 0: altimeter operating mode	0 = LRM, 1 = SAR	3a 3b 6a c2	
qual_sptr	bit 0: SPTR availability		e1	
qual_attitude	bit 1: quality of attitude	0 = ok, 1 = bad	3a 3b 6a e2 j1 j2 j3 n1 sw tx sa	
	bit 1: quality of attitude	0 = ok, 1 = suspect	g1 gs pn	
qual_dh	bit 2: dH status	1 = suspect	gs	
flag_rad_oper_mode	bit 2: TMP 21 GHz Channel status	0 = A, 1 = B	pn tx	
flag_continental_ice	bit 2: continental ice flag	0 = no, 1 = yes	3a 3b 6a c2 j1 j2 j3 n1 sw sa	
qual_iono_alt	bit 3: quality of dual-frequency iono corr	0 = ok, 1 = bad	3a 3b 6a j1 j2 j3 n1 sw tx	
flag_water	bit 4: water/dry flag	0 = open ocean or enclosed sea or lake, 1 = land	all	
flag_ocean	bit 5: ocean/land flag	0 = open ocean, 1 = land or enclosed sea or lake	all	
surface_type_rad	bit 6: radiometer land flag	0 = water, 1 = land	all but c2 gs	
qual_alt_rain_ice	bit 7: altimeter rain/ice flag	0 = no rain/ice, 1 = rain/ice	3a 3b 6a g1 j1 j2 j3 n1 pn sa sw tx	
qual_rad_rain_ice	bit 8: radiometer rain/ice flag	0 = no rain/ice, 1 = rain/ice	3a 3b 6a e1 e2 j1 j2 j3 n1 pn sw tx	
qual_rad_tb	bit 9/10: radiometer quality flag	0 = ok, 1 = interp. near land, 2 = extrap., 3 = interp. failed	pn tx	
		0 = ok, 1 = bad tb238, 2 = bad tb365, 3 = both bad	3a 3b e1 e2 n1	
		0 = ok, 1 = bad tb220, 2 = bad tb370, 3 = both bad	g1	
		0 = ok, 1 = bad tb187/tb238, 2 = bad tb340, 3 = both bad	6a j1 j2 j3 sw	
		0 = ok, 1 = bad tb238, 2 = bad tb370, 3 = both bad	sa	
qual_range	bit 11: quality of range	0 = ok, 1 = some 10Hz invalid	gs	
		0 = ok, 1 = suspect	other	
qual_swh	bit 12: quality of SSB	0 = ok, 1 = suspect	gs	
	bit 12: quality of SWH	0 = ok, 1 = suspect	other	
qual_sig0	bit 13: quality of wind speed	0 = ok, 1 = suspect	gs	
	bit 13: quality of sigma0	0 = ok, 1 = suspect	other	
flag_alt_track_mode	bit 14: altimeter tracking mode	0 = nominal, 1 = preset	e1 e2	
		0 = nominal, 1 = coarse or acquisition	gs tx	
		0 = nominal, 1 = C-band coarse	j1	
		0 = nominal, 1 = acquisition	pn	
qual_orbit	bit 15: orbital quality flag	0 = ok, 1 = suspect	all	
surface_type	surface type	0 = open ocean, 2 = enclosed sea or lake, 3 = land, 4 = continental ice	all	1
surface_class	surface class	0 = open ocean, 1 = land, 2 = continental water, 3 = aquatic vegetation, 4 = continental ice or snow, 5 = floating ice, 6 = salted basin	all	2

Notes:

1. A new variable surface_type has been introduced to combine the original flag bits 2, 4, and 5 into a single variable. Generally, the flag mask determined by flags_low as discussed above will be set to only allow data over open ocean. Effort is made to get rid of this quirky method of screening the data and use the individual flags instead.

   The values of surface_type are based on the GSHHG coastline dataset [*Wessel and Smith*, 1996] that is distributed with the Generic Mapping Tools (GMT) plotting package [*Wessel et al.*, 2013]. Version 2.3.4 of this data set was used to create land mask of ocean/land/lake indicators at 1 arcminute resolution. This grid was than queried to determine whether the satellite nadir point was over ocean, land, or lakes or enclosed seas. The additional information about continental ice came for the original GDR data. If this indicator was set in the GDR, surface_type was set to the value 4, and bits 4 and 5 of flags were both set to 1, irrespective of the aforementioned land mask.

   Experience has shown that for Antarctica only the grounded ice is marked as "continental ice" (4). The ice sheets are marked "land" (2) as the GSHHG coastline datasets marks the (minimum) extent of the ice sheets.

   The value of 1 of surface_type has been reserved for later use.

2. A more elaborate version of surface_type is available as surface_class. It fas 7 different states and is based on a high-resolution mask built from MERIS and GlobCover data.

6.2   Bathymetry and topography

Bathymetry is the depth of the oceans (and seas). It is given as a negative number, and thus constitutes the elevation of the sea bottom with respect to the geoid. The bathymetry is generally predicted from altimeter data, by inverting altimeter-derived gravity anomalies into ocean depth [*Smith and Sandwell*, 1994, e.g.].

Topography is the elevation of the land (and lakes). It is represented generally by a positive value and is measured relative to the geoid. Occasionally the values can be negative, like in large parts of The Netherlands, and around the Dead Sea. By convention, the elevation of the lake surfaces (not the lake bottom) is stored, except for the Caspian Sea for which generally the bottom topography is given. The topography models are based on a number of different sources: altimetry, the SRTM mission, and local leveling.

In RADS the bathymetry and topography are combined into a single field. Please use the surface_type variable to distinguish between ocean, land, and lakes.

Variable	name	units	sat	range	note
topo_dtm2000	DTM2000 topography	m	j1 j2 j3 n1 sa		1
topo_ace2	ACE2 topography	m	3a 3b 6a j3 sw tx pn		2
topo_srtm30plus	SRTM30PLUS topography	m	all		3
topo_srtm15plus	SRTM15PLUS topography	m	all but e1 e2 g1 gs n1		4
topo_dtu10	DTU10 topography	m	all but tx pn		5
topo	*alias of* topo_srtm15plus topo_srtm30plus		all		

Notes:

1. On some of the GDR products, the topography/bathymetry is determined from the DTM2000.1 model (N. Pavlis and J. Saleh, GSFC) and is copied into the RADS data base.

2. The topography/bathymetry model ACE2 is included on the GDR-F product standards. It is copied into the RADS data base.

3. Ocean data are based on the Smith and Sandwell global 1-minute grid between the latitudes 81°S and 81°N degrees [*Sandwell et al.*, 2014]. Higher resolution grids have been added from the LDEO Ridge Multibeam Synthesis Project, the JAMSTEC Data Site for Research Cruises, and the NGDC Coastal Relief Model. Arctic bathymetry is from the International Bathymetric Chart of the Oceans (IBCAO) [*Jakobsson et al.*, 2012].

   Land data are based on the 1-km averages of topography derived from the USGS SRTM30 gridded DEM data product created with data from the NASA Shuttle Radar Topography Mission. GTOPO30 data are used for high latitudes where SRTM data are not available.

   V10 of SRTM30_PLUS was released in May 2014. For more information about SRTM30_PLUS, please see: http://topex.ucsd.edu/WWW_html/srtm30_plus.html

   This variable is deprecated and slated for removal from the RADS data base.

4. Updated version of the global bathymetry map, adding SARAL/AltiKa, CryoSat-2, and Jason-2 altimeter data as well as increasing the resolution to 15 arc seconds [*Tozer et al.*, 2019].

5. The DTU10 topography/bathymetry model was derived from altimeter data together with the DTU10 mean sea surface model [*Andersen and Knudsen*, 2010] and is an update of the DNSC08 bathymetry model [*Andersen and Knudsen*, 2009]. It is not clear where the topographic (land) data stem from. The model is interpolated to the altimeter ground track location. **This variable is deprecated and slated for removal from the RADS data base.**

6.3   Distance from coast and coastal proximity parameter

Because the altimeter and radiometer measurements are affected by land in their respective footprints, it is worthwhile to know what the distance from the satellite nadir to any coastline is, since it would facilitate editing out of possibly corrupted measurements. RADS contains two parameters for this purpose, to be used by the user at leisure: the distance from the coast and the coastal proximity parameter. Both are based on the proximity of the altimeter footprint to land, but potentially suit different purposes.

The distance to (of from) the coast is measured from the centre of the altimeter footprint (i.e. the satellite nadir point) to the *nearest* ocean or lake shoreline. The values in the RADS data base have been interpolated in a grid with a resolution of 1 arcminute. Positive values are offshore distances to the nearest shoreline, negative values are inland distances to the nearest ocean or lake shore. The grid is based on Version 2.3.0 of the GSHHG shoreline dataset [*Wessel and Smith*, 1996] that is distributed with the Generic Mapping Tools (GMT) plotting package [*Wessel et al.*, 2013]. Any islets or lakes of less than 1 square kilometer have been excluded.

The coastal proximity parameter is a dimensionless measure of the effect of land over altimetric waveforms, and has values in the range from -1 to +1, where -1 means unaffected by land (normally offshore, open-ocean points) and 1 means totally affected by land (for instance points a few km inland). Therefore this parameter can be used for screening purposes in place of distance from coast. The grid for this parameter was developed by NOC Southampton in the framework of the ESA Sea Level CCI project and has a resolution of $0.01° \times 0.01°$ [*Cipollini*, 2011].

Variable	name	units	sat	range	note
dist_coast	distance to coast	km	all		
prox_coast	coastal proximity parameter		all		

6.4 Basin codes

Eric Leuliette (NOAA) divided the world's larger water bodies into 39 different ocean basins, enclosed seas and lakes, giving each of them a separate numerical code. This has been represented in a grid with a 5'×5' resolution as shown in Figure 6.1. This grid is queried to the nearest grid point when creating the RADS data and stored as the variable basin. For land areas a default value of NaN is stored.

This field allows users to separate the selected data by region, or select data from just a single region. Normally data from all regions is selected.

Variable	name	units	sat	range	note
basin	basin code	-	all		

6.5 Latency flag

RADS incorporates the latest available level-2 products from each mission. To distinguish the timeliness of the baseline product processed for each pass, the varlatency flag is available. By default, data from all latencies is provided.

latency	values	sat
Near-Real Time (NRT) or Operational GDR (OGDR)	0	3a 3b 6a j3 sa sw
Slow-Time Critical (STC) or Interim GDR (IGDR)	1	3a 3b 6a j3 c2 sa sw
Non-Time Critical (NTC) or "Final" GDR (GDR)	2	all except c2 sw tx pn
Reprocessed GDR-F data	3	tx pn
Reprocessing with Baseline F08	4	6a
Reprocessing with Baseline Collection 005	11	3a 3b

1 Pacific Ocean	20 Hudson Bay	41 Great Slave	60 Mediterranean
2 Atlantic Ocean	21 Gulf of Mexico	42 Lake Winipeg	61 Adriatic Sea
3 Indian Ocean	22 Caribbean Sea	43 Lake Superior	70 Black Sea
4 Arctic Ocean	23 North Sea	44 Lake Michigan	71 Caspian Sea
	24 Baltic Sea	45 Lake Huron	72 Aral Sea
10 Bering Sea	31 Arabian Sea	46 Lake Ontario	73 Lake Baikal
11 Sea of Okhotsk	32 Bay of Bengal	47 Lake Erie	74 Lake Balkhash
12 Sea of Japan	33 Andaman Sea	50 Lake Titicaca	80 Lake Chad
13 Yellow Sea	34 Persian Gulf		81 Lake Malawi
14 South China Sea	35 Red Sea		82 Lake Tanganyika
15 Indonesian			83 Lake Victoria
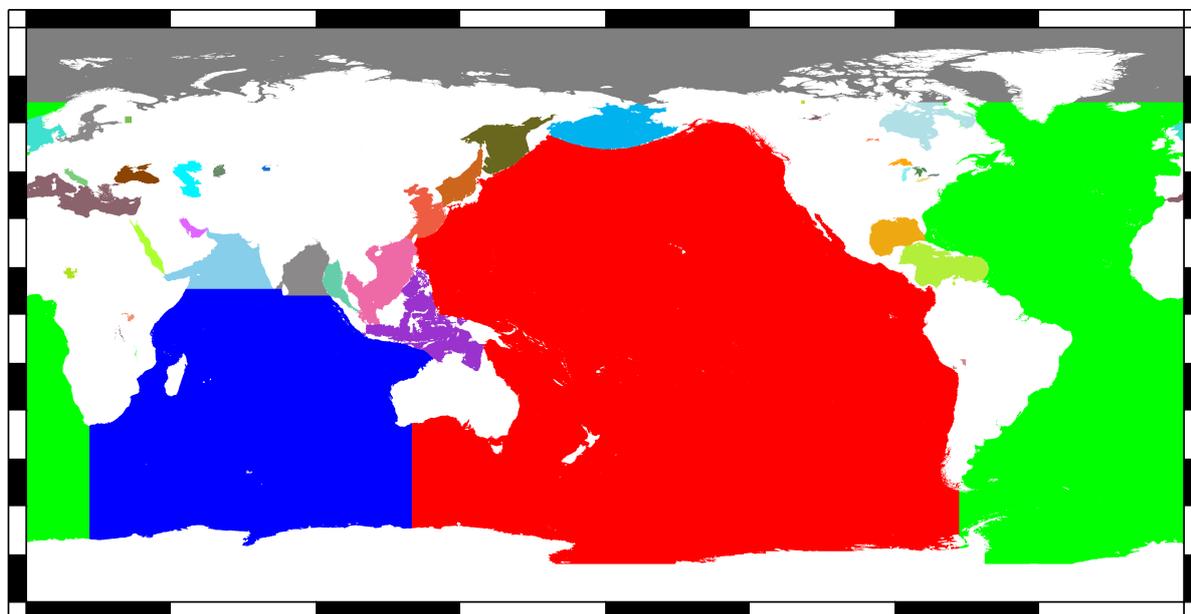
Figure 6.1   Basin codes. The different colours relate to the various numerical identifiers used for each ocean basin, enclosed sea or lake.

Bibliography

Abdalla, S. (2007), Ku-band radar altimeter surface wind speed algorithm, in *Proc. of the 2007 Envisat Symposium, Montreux, Switzerland, 23-27 April 2007, Eur. Space Agency Spec. Publ., ESA SP-636*.

Ablain, M., M.-I. Pujol, S. Philipps, and N. Picot (2008), Assessment of Jason-2 and Jason-1 orbit quality from SSH analysis, Ocean Science Topography Science Team Meeting, Nice, France, 10-12 November 2008.

Andersen, O. B., and P. Knudsen (2009), The DNSC08BAT bathymetry developed from satellite altimetry, *Tech. rep.*, Danish National Spacecenter.

Andersen, O. B., and P. Knudsen (2010), The DTU10 mean sea surface and mean dynamic topography: Improvements in the Arctic and coastal zone, Ocean Science Topography Science Team Meeting, Lisbon, Portugal, 19-21 October 2010.

Andersen, O. B., P. Knudsen, and L. Stenseng (2013), The DTU13 global mean sea surface from 20 years of satellite altimetry, Ocean Science Topography Science Team Meeting, Boulder, Colorado, 8-11 October 2013.

Andersen, O. B., P. Knudsen, and L. Stenseng (2018), A new DTU18 MSS mean sea surface – Improvement from SAR altimetry, Symposium on 25 Years of Progress in Radar Altimetry, Ponte Delgada, 24-29 September 2018.

Andersen, O. B., S. Kildegaard Rose, A. Abulaitijiang, S. Zhang, and S. Fleury (2023), The DTU21 global mean sea surface and first evaluation, *Earth Syst. Sci. Data*, *15*, 4065–4075, doi:10.5194/essd-15-4065-2023.

Argus, D. F., and R. S. Gross (2004), An estimate of motion between the spin axis and the hotspots over the past century, *Geophys. Res. Lett.*, *31*, L06614, doi:doi:10.1029/2004GL019657.

Askne, J., and H. Nordius (1987), Estimation of tropospheric delay for microwaves from surface weather data, *Radio Sci.*, *22*(3), 379–386, doi:10.1029/RS022i003p00379.

AVISO (2021), MSS combined SIO/CNES_CLS2015/DTU15, *Tech. Rep. SALP-MU-P-EA-23489-CLS*, Aviso+ Altimetry, Ramonville St. Agne, France, doi:10.24400/527896/a01-2021.004.

Berrisford, P., et al. (2011), The ERA-interim archive Version 2.0, *ERA Report Series 1*, ECMWF, Reading, UK.

Bevis, M., S. Businger, S. Chriswell, T. A. Herring, R. A. Anthes, C. Rocken, and R. H. Ware (1994), GPS meteorology: Mapping zenith wet delays onto precipitable water, *J. Appl. Meteor.*, *33*(3), 379–386, doi:10.1175/1520-0450(1994)033$\langle$0379:GMMZWD$\rangle$2.0.CO;2.

Bignalet-Cazalet, F., A. Couhert, N. Queruel, S. Urien, L. Carrère, N. Tran, and G. Jettou (2021), SARAL/AltiKa products handbook, *SALP-MU-M-OP-15984-CN, issue 3.1*, CNES and ISRO, doi:SARAL.

Bouffard, J. (2015), CryoSat-2: Level 2 products evolutions and quality improvements in Baseline C, *XCRY-GSEG-EOPG-TN-15-0004*, ESA.

Carrère, L., and F. Lyard (2003), Modeling the barotropic response of the global ocean to atmospheric wind and pressure forcing - comparisons with observations, *Geophys. Res. Lett.*, *30*(6), doi:10.1029/2002GL016473.

Carrère, L., Y. Faugère, and M. Ablain (2016), Major improvement of altimetry sea level estimations using pressure derived corrections based on ERA-interim atmospheric reanalysis, *Ocean Sci. Discuss.*, *12*, 825–842, doi:10.5194/os-12-825-2016.

Cartwright, D. E., and A. C. Edden (1973), Corrected tables of tidal harmonics, *Geophys. J. Roy. Astron. Soc.*, *33*, 253–264, doi:10.1111/j.1365-246X.1973.tb03420.x.

Cartwright, D. E., and R. J. Taylor (1971), New computations of the tide-generating potential, *Geophys. J. Roy. Astron. Soc.*, *23*, 45–74, doi:10.1111/j.1365-246X.1971.tb01803.x.

Chawla, A., D. Spindler, and H. L. Tolman (2011), WAVEWATCH III hindcasts with re-analysis winds: Initial report on model setup, *MMAB Contribution No. 291*, NOAA National Weather Service, Camp Springs, Maryland.

Chelton, D. B. (1994), The sea state bias in altimeter estimates of sea lvel from collinear analysis of TOPEX data, *J. Geophys. Res.*, *99*(C12), 24,995–25,008.

Cheney, R. E., N. S. Doyle, B. C. Douglas, R. W. Agreen, L. Miller, E. L. Timmerman, and D. C. McAdoo (1991), The complete Geosat altimeter GDR handbook, *NOAA Tech. Memo. NOS NGS-7*, National Ocean Service, Rockville, Maryland.

Cipollini, P. (2011), A new parameter to facilitate screening of coastal altimetry data and corrections, Ocean Science Topography Science Team Meeting, San Diego, 19-21 October 2011.

Collard, F. (2005), Algorithmes de vent et periode moyenne des vagues JASON a base de reseaux de neurons, *Rapport BO-021-CLS-0407-RF*, Boost Technologies.

Crétaux, J.-F., and C. M. Birkett (2006), Lake studies from satellite radar altimetry, *C. R. Geoscience*, *338*, 1098–1112, doi:10.1016/j.crte.2006.08.002.

Desai, S. D., J. M. Wahr, and B. D. Beckley (2015), Revisiting the pole tide for and from satellite altimetry, *J. Geod.*, *89*(12), 1233–1243, doi:10.1007/s00190-015-0848-7.

Dumont, J.-P., P. Sicard, J. Stum, and O.-Z. Zanifé (2001), Algorithm definition, accuracy and specification volume 4: CMA altimeter level 2 processing, *Tech. Rep. SMM-ST-M2-EA-11005-CN*, CNES/SSALTO.

Feng, H., S. Yao, L. Li, N. Tran, D. Vandemark, and S. Labroue (2010), Spline-based nonparametric estimation of the altimeter sea state bias correction, *IEEE Geosci. Rem. Sens. Lett.*, *7*(3), 577–581.

Förste, C., et al. (2013), EIGEN-6C3stat – the newest high resolution global combined gravity field model based on the 4th release of the GOCE direct approach, *Tech. rep.*, ICGEM/GFZ Postdam.

Francis, C. R. (1990), The ERS-1 radar altimeter, paper presented at the 2nd ERS-1 PI meeting, Noordwijk,The Netherlands.

Francis, C. R., et al. (1993), The Calibration of the ERS-1 Radar Altimeter – The Venice Calibration Campaign, *ESA Report ER-RP-ESA-RA-0257 issue 2.0*, ESA/ESTEC, Noordwijk,The Netherlands.

Francis, C. R., et al. (1995), The ERS-2 spacecraft and its payload, *ESA Bulletin*, *83*, 13–31.

Francis, C. R., et al. (1991), The ERS-1 spacecraft and its payload, *ESA Bulletin*, *65*, 26–48.

Gaspar, P., and J.-P. Florens (1998), Estimation of the sea state bias in radar altimeter measurements of sea level: Results from a new nonparametric method, *J. Geophys. Res.*, *103*(C8), 15,803–15,814.

Gaspar, P., F. Ogor, P.-Y. Le Traon, and O.-Z. Zanifé (1994), Estimating the sea state bias of the TOPEX and POSEIDON altimeters from crossover differences, *J. Geophys. Res.*, *99*(C12), 24,981–24,994.

Gaspar, P., S. Labroue, F. Ogor, G. Lafitte, L. Marchal, and M. Rafanel (2002), Improving nonparametric estimates of the sea state bias in radar altimeter measurements of sea level, *J. Atmos. Oceanic Technol.*, *19*(10), 1690–1707.

Gourrion, J., D. Vandemark, S. Bailey, B. Chapron, C. P. Gommenginger, P. G. Challenor, and M. A. Srokosz (2002), A two-parameter wind speed algorithm for Ku-band altimeters, *J. Atmos. Oceanic Technol.*, *19*(12), 2030–2048, doi:10.1175/1520-0426(2002)019$\langle$2030:ATPWSA$\rangle$2.0.CO;2.

International DORIS Service (2011), New GDR-D orbit standards, ftp://ftp.ids-doris.org/pub/ids/data/POD_configuration_GDRD.pdf (retrieved 25 June 2015).

International DORIS Service (2015), New GDR-E orbit standards, ftp://ftp.ids-doris.org/pub/ids/data/POD_configuration_GDRE.pdf (retrieved 25 June 2015).

Jakobsson, M., et al. (2012), The International Bathymetric Chart of the Arctic Ocean (IBCAO) version 3.0, *Geophys. Res. Lett.*, *39*, L12609, doi:10.1029/2012GL052219.

Keihm, S. J., M. A. Janssen, and C. S. Ruf (1995), TOPEX microwave radiometer (TMR): III. Wet troposphere range correction algorithm and pre-launch error budget, *IEEE Trans. Geosci. Rem. Sens.*, *33*(1), 147–161.

Komjathy, A., G. H. Born, and D. N. Anderson (2000), An improved high precision ionospheric total electron content modeling using GPS, in *Proc. International Geoscience and Remote Sensing Symposium (IGARSS), Honolulu, Hawaii, 2000*, vol. 7, pp. 2858–2860, doi:10.1109/IGARSS.2000.86027.

Labroue, S., and E. Obligis (2003), Neural network retrieval algorithms for the Envisat/MWR, *Tech. Rep. CLS/DOS/NT/03.848*, Collect., Localisation, Satell., Ramonville St. Agne, France.

Labroue, S., P. Gaspar, J. Dorandeu, O.-Z. Zanifé, F. Mertz, P. Vincent, and D. Choquet (2004), Nonparametric estimates of the sea state bias for the Jason-1 radar altimeter, *Mar. Geod.*, *27*(3-4), 453–481, doi:10.1080/01490410490902089.

Lambin, J., et al. (2010), The OSTM/Jason-2 mission, *Mar. Geod.*, *33*(S1), 4–25, doi:10.1080/01490419.2010.491030.

Lemoine, F. G., N. P. Zelensky, D. S. Chinn, B. D. Beckley, and J. L. Lillibridge (2006), Towards the GEOSAT Follow-On precise orbit determination goals of high accuracy and near-real-time processing, paper 2006-6402, AIAA/AAS Astrodynamics Specialist Conference, August 21–24, 2006, Keystone, Colorado.

Lemoine, F. G., N. P. Zelensky, S. A. Melachroinos, D. S. Chinn, and B. D. Beckley (2013), Status of the GSFC precise orbit ephemerides for Jason-2, Jason-1 and TOPEX/Poseidon, Ocean Science Topography Science Team Meeting, Boulder, Colorado, 8-11 October 2013.

Lillibridge, J. L., R. Scharroo, S. Abdalla, and D. C. Vandemark (2014), One- and two-dimensional wind speed models for Ka-band altimetry, *J. Atmos. Oceanic Technol.*, *31*(3), 630–638, doi:10.1175/JTECH-D-13-00167.1.

Llewellyn, S. K., and R. B. Bent (1973), Documentation and description of the Bent ionospheric model, *Rep. AFCRL-TR-73-0657*, Air Force Cambridge Research Laboratory, Hanscom Air Force Base, Massachusetts.

Lyard, F., F. Lefèvre, T. Letellier, and O. Francis (2006), Modelling the global ocean tides: modern insights from FES2004, *Ocean Dynamics*, *56*(5-6), 394–415, doi:10.1007/s10236-006-0086-x.

Martini, A., and P. Féménias (2000), The ERS SPTR2000 altimeric range correction: Results and validation, *Technical Note ERE-TN-ADQ-GSO-6001*, ESA/ESRIN, Frascati, Italy.

Ménard, Y., L.-L. Fu, P. Escudier, B. J. Haines, G. Kunstmann, F. Parisot, J. Perbos, P. Vincent, and S. D. Desai (2003), The Jason-1 mission, *J. Mar. Geod.*, *Jason-1*.

Mendes, V. B., G. Prates, L. Santos, and R. B. Langley (2000), An evaluation of the accuracy of models for the determination of the weighted mean temperature of the atmosphere, in *Proc. of the 2000 National Technical Meeting of The Institute of Navigation, Anaheim, CA, January 2000*, pp. 433–438.

Munk, W. H., and G. J. F. MacDonald (1960), *The Rotation of the Earth: A Geophysical Discussion*, Cambridge University Press, New York.

Pavlis, N. K., S. A. Holmes, S. C. Kenyon, and J. K. Factor (2012), The development and evaluation of the Earth Gravitational Model 2008 (EGM2008), *J. Geophys. Res.*, *117*, B04406, doi:10.1029/2011JB008916.

Ponte, R. M., and R. D. Ray (2002), Atmospheric pressure corrections in geodesy and oceanography: A strategy for handling air tides, *Geophys. Res. Lett.*, *29*(24), 2153–2156, doi:10.1029/2002GL016340.

Putnam Shileah, A. A. (2021), *ea state bias model development and error analysis for pulse-limited altimetry*, Ph.D. thesis, University of Colorado, Boulder, Colorado.

Quartly, G. D. (2009), Optimizing σ^0 information from Jason-2 altimeter, *IEEE Geosci. Rem. Sens. Lett.*, *6*(3), 398–402, doi:10.1109/LGRS.2009.2013973.

Ray, R. D. (2013), Precise comparisons of bottom-pressure and altimetric ocean tides, *J. Geophys. Res.*, *118*, 4570–4584, doi:10.1002/jgrc.20336.

Ray, R. D., and E. D. Zaron (2016), M_2 internal tide and their observed wavenumber from satellite altimetry, *J. Phys. Oceanogr.*, *46*(3-22), doi:10.1175/JPO-D-15-0065.1.

Ray, R. D., G. D. Egbert, and S. Y. Erofeeva (2011), Tide predictions in shelf and coastal waters: status and prospects, in *Coastal Altimetry*, edited by S. Vignudelli, A. Kostianoy, P. Cipollini, and J. Benveniste, Springer-Verlag.

Roblou, L., F. Lyard, J. Dorandeu, J. Lamouroux, and J. Bouffard (2008), Dealiasing high frequency ocean response to atmospheric forcing, presented at the Coastal Altimetry Workshop, Silver Spring, Maryland, 5-7 Feb 2008.

Rosmorduc, V., H. Roinard, S. D. Desai, J. D. Desjonqueres, P. S. Callahan, and F. Bignalet-Cazalet (2023), TOPEX/Poseidon GDR-F products handbook, *JPL D-73899/SALP-MY-MAO-DP-17607-CN*, NASA/JPL and CNES.

Rudenko, S., M. Otten, P. N. A. M. Visser, R. Scharroo, and T. Schöne (2011), Improvements in ERS-1 and ERS-2 precise orbit determination, Poster presentation at EGU 2011 General Assembly.

Rudenko, S., D. Dettmering, S. Esselborn, T. Schöne, C. Förste, J.-M. Lemoine, M. Ablain, D. Alexandre, and K.-H. Neumayer (2014), Influence of time variable geopotential models on precise orbits of altimetry satellites, global and regional mean sea level trends, *Adv. Space Res.*, *54*(1), 92–118, doi:10.106/j.asr.2014.03.010.

Rudenko, S., K.-H. Neumayer, D. Dettmering, S. Esselborn, T. Schöne, and J. C. Raimondo (2015), New orbits of ERS-1, ERS-2, TOPEX/Poseidon, Envisat, Jason-1 and Jason-2 for altimetry applications and their validation, Ocean Science Topography Science Team Meeting, Reston, Virginia, 20-23 October 2015.

Rudenko, S., K.-H. Neumayer, D. Dettmering, S. Esselborn, T. Schöne, and J. C. Raimondo (2016), Improvements in precise orbits of altimetry satellites and their altimetry validation, (under preparation).

Ruf, C. S., R. P. Dewan, and B. Sabramanya (1996), Combined microwave radiometer and altimeter retrieval of wet path delay for Geosat Follow-On, *IEEE Trans. Geosci. Rem. Sens.*, *34*(4), 991–999.

Saastamoinen, J. (1972), Atmospheric corrections for the troposphere and stratosphere in radio ranging of satellites, in *The Use of Artificial Satellites for Geodesy*, *Geophys. Monogr. Ser.*, vol. 15, edited by S. W. Hendriksen, A. Mancini, and B. H. Chovitz, pp. 247–251, American Geophysical Union, Washington, D.C.

Sandwell, D. T., R. D. Müller, W. H. F. Smith, E. S. Garcia, and C. R. Francis (2014), New global marine gravity model from CryoSat-2 and Jason-1 reveals buried tectonic structure, *Science*, *346*(6205), 65–67, doi:10.1126/science.1258213.

Schaeffer, P., Y. Faugère, J.-F. Legeais, A. Ollivier, T. Guinle, and N. Picot (2012), The CNES-CLS11 global mean sea surface computed from 16 years of satellite altimeter data, *Mar. Geod.*, *35*(sup1), 3–19, doi:10.1080/01490419.2012.718231.

Schaeffer, P., M.-I. Pujol, P. Veillard, Y. Faugère, Q. Dagneaux, G. Dibarboure, and N. Picot (2023), The CNES CLS 2022 mean sea surface: Short wavelength improvements from CryoSat-2 and SARAL/AltiKa high-sampled altimeter data, *Remote Sens.*, *15*, 2910, doi: 10.3390/rs15112910.

Scharroo, R., and J. L. Lillibridge (2005), Non-parametric sea-state bias models and their relevance to sea level change studies, in *Proceedings of the 2004 Envisat & ERS Symposium, Eur. Space Agency Spec. Publ., ESA SP-572*, edited by H. Lacoste and L. Ouwehand.

Scharroo, R., and W. H. F. Smith (2010), A global positioning system-based climatology for the total electron content in the ionosphere, *J. Geophys. Res.*, *115*(A10318), doi:10.1029/2009JA014719.

Scharroo, R., and P. N. A. M. Visser (1998), Precise orbit determination and gravity field improvement for the ERS satellites, *J. Geophys. Res.*, *103*(C4), 8113–8127, doi:10.1029/97JC03179.

Shako, R., C. Förste, O. Abrikosov, S. Bruinsma, J. C. Marty, J.-M. Lemoine, F. Flechtner, K.-H. Neumayer, and C. Dahle (2014), EIGEN-6C: A high-resolution global gravity combination model including GOCE data, in *Observation of the System Earth from Space - CHAMP, GRACE, GOCE and future missions*, edited by F. Flechtner, N. Sneeuw, and W.-D. Schuh, Advanced Technologies in Earth Sciences, pp. 155–161, Springer Berlin Heidelberg, doi: 10.1007/978-3-642-32135-1_20.

Smith, W. H. F., and D. T. Sandwell (1994), Bathymetric prediction from dense satellite altimetry and sparse shipboard bathymetry, *J. Geophys. Res.*, *99*(B11), 21,803–21,824.

Stammer, D., et al. (2014), Accuracy assessment of global barotropic ocean tide models, *Rev. Geophys.*, *52*(3), 243–282, doi:10.1002/2014RG000450.

Stenseng, L., G. Piccioni, O. B. Andersen, and P. Knudsen (2015), Sea surface retracking and classification of cryosat-2 altimetry observations in the arctic ocean, presented at AGU 2015 Fall Meeting.

Stum, J., F. Ogor, P.-Y. Le Traon, J. Dorandeu, P. Gaspar, and J.-P. Dumont (1998), An intercal-ibration study of TOPEX, ERS-1 and ERS-2 altimetric missions: Final report of IFREMER contract No. 97/2 426 086/C, *Tech. Rep. CLS/DOS/NT/98.070*, Collect., Localisation, Satell., Ramonville St. Agne, France.

Tamura, Y. (1987), A harmonic development of the tide-generating potential, *Bull. d'Inform. Marées Terr.*, *99*, 6813–6855.

Tapley, B. D., M. M. Watkins, J. C. Ries, G. W. Davis, R. J. Eanes, S. R. Poole, H. J. Rim, B. E. Schutz, and C.-K. Shum (1996), The Joint Gravity Model 3, *J. Geophys. Res.*, *101*(B12), 28,029–28,049.

Tolman, H. L. (2009), User manual and system documentation of WAVEWATCH III version 3.14, *Tech. rep.*, NOAA National Weather Service.

Tozer, B., D. T. Sandwell, W. H. F. Smith, C. Olsen, J. R. Beale, and P. Wessel (2019), Global bathymetry and topography at 15 arc sec: SRTM15+, *Earth and Space Science*, *6*, doi:10.1029/2019EA000658.

Tran, N., D. Vandemark, S. Labroue, H. Feng, B. Chapron, H. L. Tolman, J. Lambin, and N. Picot (2010), Sea state bias in altimeter sea level estimates determined by combining wave model and satellite data, *J. Geophys. Res.*, *115*, C03020, doi:10.1029/2009JC005534.

Tran, N., S. Philipps, J. C. Poisson, S. Urien, E. Bronner, and N. Picot (2012), Impact of GDR-D standards on SSB correction, Ocean Science Topography Science Team Meeting, Venice, Italy, 27-29 September 2012.

Tran, N., D. Vandemark, E. D. Zaron, P. Thibaut, G. Dibarboure, and N. Picot (2021), Assessing the effects of sea-state related errors on the precision of high-rate Jason-3 altimeter sea level data, *Adv. Space Res.*, *68*(2), 963–977, doi:10.1016/j.asr.2019.11.034.

Wahr, J. M. (1985), Deformation of the Earth induced by polar motion, *J. Geophys. Res.*, *90*(B11), 9363–9368, doi:10.1029/JB090iB11p09363.

Wahr, J. M., R. S. Nerem, and S. V. Bettadpur (2015), The pole tide and its effect on GRACE time-variable gravity measurements: implications for the estimates of surface mass varia-tions, *J. Geophys. Res.*, *120*, 4597–4615, doi:10.1002/2015JB011986.

Wessel, P., and W. H. F. Smith (1996), A global, self-consistent, hierarchical, high-resolution shoreline, *J. Geophys. Res.*, *101*(B4), 8741–8743.

Wessel, P., W. H. F. Smith, R. Scharroo, J. Luis, and F. Wobbe (2013), Generic Mapping Tools: Improved version released, *Eos Trans. AGU*, *94*(45), 409–410, doi:10.1002/2013EO450001.

Witter, D. L., and D. B. Chelton (1991), A Geosat altimeter wind speed algorithm and a method for altimeter wind speed algorithm development, *J. Geophys. Res.*, *96*(C5), 8853–8860.

Zaron, E. D. (2019), Baroclinic tidal sea level from exact-repeat mission altimetry, *J. Phys. Oceanogr.*, *49*(1), 193–210, doi:10.1175/JPO-D-18-0127.1.

Index